Structure of the Intermediate Phase Glasses GeSe$_3$ and GeSe$_4$: The Deployment of Neutron Diffraction With Isotope Substitution

Ruth F. Rowlands[1], Anita Zeidler[1,2], Henry E. Fischer[3] and Philip S. Salmon[1,2]*

[1] Department of Physics, University of Bath, Bath, United Kingdom, [2] Science and Technology Division, Corning Incorporated, Corning, NY, United States, [3] Diffraction Group, Institut Laue Langevin, Grenoble, France

The method of neutron diffraction with isotope substitution was used to measure the full set of partial pair-correlation functions for each of the network-forming glasses GeSe$_3$ and GeSe$_4$, which lie at the boundaries of the so-called intermediate phase in the Ge-Se system. The results show the formation of chemically ordered networks, where selenium chains are cross-linked by Ge(Se$_4$)$_{1/2}$ tetrahedra, in contrast to glassy GeSe$_2$ where the chemical order is broken. In all of these materials, the Ge-centered structural motifs are distributed unevenly on an intermediate length scale, as indicated by the appearance of a first sharp diffraction peak in the Bhatia-Thornton concentration-concentration partial structure factor. The new experimental work provides benchmark results for guiding in the development of realistic structural models, which can be used to explore the network rigidity and other structure-related properties of the glass. In this context, there are discrepancies between experiment and the predictions of first-principles molecular dynamics simulations that are particularly marked in respect of the Ge-Ge correlation functions, which are sensitive to the connectivity of the Ge-centered structural motifs.

Keywords: chalcogenide glass, glass structure, neutron diffraction, rigidity percolation, intermediate phase

1. INTRODUCTION

The Ge$_x$Se$_{1-x}$ ($0 \leq x \leq 1$) system is a prototype for understanding the atomic-scale organization in covalently-bonded network glass-forming materials (Tronc et al., 1973; Bresser et al., 1986; Sugai, 1987; Penfold and Salmon, 1991; Zhou et al., 1991; Salmon and Liu, 1994; Feng et al., 1997; Wang et al., 1998; Petri et al., 1999a,b, 2000; Bureau et al., 2003; Salmon and Petri, 2003; Salmon, 2007a; Sartbaeva et al., 2007; Shatnawi et al., 2008; Inam et al., 2009; Lucas et al., 2009; Gjersing et al., 2010a,b; Bauchy et al., 2011; Hosokawa et al., 2011; Micoulaut et al., 2013; Salmon and Zeidler, 2015; Kaseman et al., 2016; Zeidler et al., 2017; Whittaker et al., 2018), where the network-forming motifs provide some of the essential building-blocks for technologically relevant chalcogenide glasses (Hilton, 1966; Seddon and Laine, 1997; Zakery and Elliott, 2003, 2007; Gopinath et al., 2004; Lezal et al., 2004; Kohoutek et al., 2008; Troles et al., 2009; Eggleton et al., 2011). According to mean-field constraint-counting theory, the glass network will undergo the transition with increasing x from an under-constrained elastically floppy phase to an over-constrained stressed-rigid phase at $x = 0.2$, where the mean number of Lagrangian bonding constraints per atom $\bar{N}_c = 3$, the number of degrees of freedom per atom in three dimensions (Phillips, 1979; Thorpe, 1983). At the $x = 0.2$ composition the mean nearest-neighbor coordination number $\bar{n} = 2.4$. In comparison,

spectroscopic and calorimetric measurements on the Ge_xSe_{1-x} system suggest that the floppy and stressed-rigid phases are separated by an 'intermediate phase' that extends over the finite composition range $0.20 \leq x \leq 0.26$ (Boolchand et al., 2001a,b; Bhosle et al., 2011, 2012). For this range, it is argued that the system lowers its free energy on glass formation by self-organizing to incorporate structural configurations that minimize the occurrence of either over or under constrained regions, to give a glass network that is isostatically rigid and stress-free (Thorpe et al., 2000). Here, self-organization is facilitated by structural variability, i.e., an ability of the system to accommodate different atomic conformations (Sartbaeva et al., 2007; Massobrio et al., 2009). The intermediate phase should therefore have a structural origin, but its signature has not been identified from diffraction or extended X-ray absorption fine structure (EXAFS) spectroscopy experiments (Shatnawi et al., 2008; Zeidler et al., 2017), or from molecular dynamics simulations (Micoulaut et al., 2013). From a dynamical perspective in the Ge_xSe_{1-x} system, intermediate phase compositions correspond to a maximum in the viscosity at the liquidus temperature, and to a minimum in the fragility index (Zeidler et al., 2017).

In this paper we take advantage of recent advances in neutron diffraction instrumentation to investigate the structure of two glasses that delimit the intermediate phase. Specifically, neutron diffraction with isotope substitution (NDIS) (Fischer et al., 2006; Salmon and Zeidler, 2013) is combined with singular valued decomposition (SVD) (Ludwig et al., 1987; Zeidler et al., 2010) to measure the full set of partial structure factors for glassy $GeSe_3$ ($x = 0.25$) and $GeSe_4$ ($x = 0.20$). These structure factors represent the maximal information that can be extracted from experiment at the pair-correlation function level. The results are compared to those obtained from high resolution ^{77}Se magic angle spinning (MAS) nuclear magnetic resonance (NMR) (Gjersing et al., 2010b) or two-dimensional ^{77}Se NMR (Kaseman et al., 2016) spectroscopy. The results are also compared to those obtained from recent density-functional-theory based first-principles molecular dynamics (FPMD) simulations (Kibalchenko et al., 2011; Bouzid and Massobrio, 2012; Micoulaut et al., 2013; Wezka et al., 2014; Bouzid et al., 2015; Chaker et al., 2018). This simulation approach is favored when modeling the structure of materials in the Ge_xSe_{1-x} system on account of the similarity between the electronegativity values for Ge and Se, although there are issues regarding the sensitivity of FPMD models to the size of the simulated system, and to the protocol used to prepare a glass from the liquid state (Bouzid et al., 2015; Le Roux et al., 2016).

The paper is organized as follows. The essential theory for the NDIS experiments is given in section 2. The experimental methods are then described in section 3, where the choice of neutron diffractometer enabled the diffraction patterns to be measured with excellent count-rate stability over a wide range of scattering vectors. The results are presented in section 4 at both the first-difference function and partial structure factor levels in order to check for self-consistency in the measured parameters. The results are discussed in section 5 by reference to those obtained from other experiments and FPMD simulations, where issues include the nature and connectivity of the structural

motifs, and whether there is a structural signature of the intermediate phase (Shatnawi et al., 2008; Zeidler et al., 2017). Conclusions are drawn in section 6.

2. THEORY

In a neutron diffraction experiment on glassy $GeSe_3$ or $GeSe_4$, the total structure factor (Fischer et al., 2006)

$$F(k) = \sum_\alpha \sum_\beta c_\alpha c_\beta b_\alpha b_\beta \left[S_{\alpha\beta}(k) - 1 \right], \qquad (1)$$

is measured, where α and β denote the chemical species, c_α and b_α represent the atomic fraction and coherent neutron scattering length of chemical species α, respectively, $S_{\alpha\beta}(k)$ is a Faber-Ziman (Faber and Ziman, 1965) partial structure factor, and k is the modulus of the scattering vector. Consider the case of four samples that are identical in every respect, except for their isotopic compositions. Let the Ge-Se isotope combinations be represented by nat-nat, nat-mix, 70-nat, and 73–76, where nat denotes the natural isotopic abundance and mix denotes a mixture of Se isotopes, with enrichments (see section 3.1) that give coherent scattering lengths of $b_{natGe} = 8.185(20)$, $b_{70Ge} = 9.93(10)$, $b_{73Ge} = 5.16(4)$, $b_{natSe} = 7.970(9)$, $b_{mixSe} = 10.10(5)$, and $b_{76Se} = 12.19(10)$ fm (Sears, 1992). Then, if the total structure factors are denoted by $^{nat}_{nat}F(k)$, $^{nat}_{mix}F(k)$, $^{70}_{nat}F(k)$, and $^{73}_{76}F(k)$, respectively, it follows that

$$\begin{pmatrix} ^{nat}_{nat}F(k) \\ ^{nat}_{mix}F(k) \\ ^{70}_{nat}F(k) \\ ^{73}_{76}F(k) \end{pmatrix} = \mathbf{W} \begin{pmatrix} S_{GeGe}(k) - 1 \\ S_{SeSe}(k) - 1 \\ S_{GeSe}(k) - 1 \end{pmatrix}. \qquad (2)$$

In the case of $GeSe_3$ the weighting factor matrix is given by

$$\frac{\mathbf{W}}{barn} = \begin{pmatrix} 0.0419(2) & 0.3573(8) & 0.2446(8) \\ 0.0419(2) & 0.574(6) & 0.310(2) \\ 0.0616(12) & 0.3573(8) & 0.297(4) \\ 0.0166(2) & 0.836(14) & 0.236(4) \end{pmatrix} \qquad (3)$$

(1 barn $= 10^{-28}$ m^2), and in the case of $GeSe_4$ the weighting factor matrix is given by

$$\frac{\mathbf{W}}{barn} = \begin{pmatrix} 0.0268(1) & 0.4065(9) & 0.2088(7) \\ 0.0268(1) & 0.653(7) & 0.265(2) \\ 0.0394(8) & 0.4065(9) & 0.253(3) \\ 0.0106(2) & 0.951(16) & 0.201(3) \end{pmatrix}. \qquad (4)$$

The partial structure factors $S_{\alpha\beta}(k)$ are related to the partial pair-distribution functions $g_{\alpha\beta}(r)$ via the Fourier transform relation

$$g_{\alpha\beta}(r) = 1 + \frac{1}{2\pi^2 \rho r} \int_0^\infty dk\, k \left[S_{\alpha\beta}(k) - 1 \right] \sin(kr) \qquad (5)$$

where ρ is the atomic number density and r is a distance in real space. The mean coordination number of atoms of type β,

contained in a volume defined by two concentric spheres of radii r_1 and r_2 centered on an atom of type α, is given by

$$\bar{n}_\alpha^\beta = 4\pi \, \rho \, c_\beta \int_{r_1}^{r_2} \mathrm{d}r \, r^2 g_{\alpha\beta}(r). \qquad (6)$$

It is possible to eliminate one of the partial structure factors by combining two total structure factors. For example, $S_{\mathrm{SeSe}}(k)$ can be eliminated by forming a first-difference function such as

$$
\begin{aligned}
\Delta F_{\mathrm{Ge}}(k) &\equiv {}^{70}_{\mathrm{nat}}F(k) - \left(b^2_{\mathrm{nat\,Se}} \,/\, b^2_{76\,\mathrm{Se}}\right) {}^{73}_{76}F(k) \\
&= c^2_{\mathrm{Ge}} \left(b^2_{70\,\mathrm{Ge}} - b^2_{73\,\mathrm{Ge}} b^2_{\mathrm{nat\,Se}} \,/\, b^2_{76\,\mathrm{Se}}\right) \left[S_{\mathrm{GeGe}}(k) - 1\right] \\
&\quad + 2 c_{\mathrm{Ge}} c_{\mathrm{Se}} \left(b_{70\,\mathrm{Ge}} b_{\mathrm{nat\,Se}} - b_{73\,\mathrm{Ge}} b^2_{\mathrm{nat\,Se}} \,/\, b_{76\,\mathrm{Se}}\right) \\
&\quad \left[S_{\mathrm{GeSe}}(k) - 1\right].
\end{aligned}
\qquad (7)
$$

Similarly, $S_{\mathrm{GeSe}}(k)$ can be eliminated by forming a first-difference function such as

$$
\begin{aligned}
\Delta F(k) &\equiv {}^{73}_{76}F(k) - \left(b_{73\,\mathrm{Ge}} b_{76\,\mathrm{Se}} \,/\, b_{70\,\mathrm{Ge}} b_{\mathrm{nat\,Se}}\right) {}^{70}_{\mathrm{nat}}F(k) \\
&= c^2_{\mathrm{Ge}} \left(b^2_{73\,\mathrm{Ge}} - b_{70\,\mathrm{Ge}} b_{73\,\mathrm{Ge}} b_{76\,\mathrm{Se}} \,/\, b_{\mathrm{nat\,Se}}\right) \left[S_{\mathrm{GeGe}}(k) - 1\right] \\
&\quad + c^2_{\mathrm{Se}} \left(b^2_{76\,\mathrm{Se}} - b_{73\,\mathrm{Ge}} b_{\mathrm{nat\,Se}} b_{76\,\mathrm{Se}} \,/\, b_{70\,\mathrm{Ge}}\right) \left[S_{\mathrm{SeSe}}(k) - 1\right].
\end{aligned}
\qquad (8)
$$

The corresponding real-space functions, denoted by $\Delta G_{\mathrm{Ge}}(r)$ and $\Delta G(r)$, are obtained from Equations (7) and (8), respectively, by replacing each $S_{\alpha\beta}(k)$ by the corresponding $g_{\alpha\beta}(r)$ function. The weighting factors for the Ge-Ge and Ge-Se partial structure factors in Equation (7) are 0.054(1) and 0.196(3) barn for GeSe$_3$ vs. 0.0349(8) and 0.167(3) barn for GeSe$_4$, respectively. The weighting factors for the Ge-Ge and Se-Se partial structure factors in Equation (8) are $-0.0323(6)$ and 0.552(12) barn for GeSe$_3$ vs. $-0.0207(4)$ and 0.628(14) barn for GeSe$_4$, respectively. The first-difference functions are obtained from pairs of measured $F(k)$ functions, whereas the partial structure factors are obtained by combining all of the measured $F(k)$ functions. Self-consistent results are expected if systematic errors are small (Salmon and Petri, 2003).

It is also informative to decompose a total structure factor into its contributions from the Bhatia-Thornton (Bhatia and Thornton, 1970) number-number, concentration-concentration, and number-concentration partial structure factors denoted by $S_{\mathrm{NN}}(k)$, $S_{\mathrm{CC}}(k)$ and $S_{\mathrm{NC}}(k)$, respectively, where

$$
\begin{aligned}
F(k) = \langle b\rangle^2 \left[S_{\mathrm{NN}}(k) - 1\right] + c_{\mathrm{Ge}} c_{\mathrm{Se}} (b_{\mathrm{Ge}} - b_{\mathrm{Se}})^2 \big\{\left[S_{\mathrm{CC}}(k) \,/\, c_{\mathrm{Ge}} c_{\mathrm{Se}}\right] \\
- 1\big\} + 2\langle b\rangle (b_{\mathrm{Ge}} - b_{\mathrm{Se}}) S_{\mathrm{NC}}(k)
\end{aligned}
\qquad (9)
$$

and $\langle b\rangle = c_{\mathrm{Ge}} b_{\mathrm{Ge}} + c_{\mathrm{Se}} b_{\mathrm{Se}}$ is the mean coherent scattering length. Equation (2) can then be re-written as

$$
\begin{pmatrix} {}^{\mathrm{nat}}_{\mathrm{nat}}F(k) \\ {}^{\mathrm{nat}}_{\mathrm{mix}}F(k) \\ {}^{70}_{\mathrm{nat}}F(k) \\ {}^{73}_{76}F(k) \end{pmatrix} = \mathbf{W}' \begin{pmatrix} S_{\mathrm{NN}}(k) - 1 \\ \left[S_{\mathrm{CC}}(k) \,/\, c_{\mathrm{Ge}} c_{\mathrm{Se}}\right] - 1 \\ S_{\mathrm{NC}}(k) \end{pmatrix}, \qquad (10)
$$

where in the case of GeSe$_3$ the weighting factor matrix is given by

$$
\frac{\mathbf{W}'}{\mathrm{barn}} = \begin{pmatrix} 0.644(1) & 0.00009(2) & 0.035(1) \\ 0.926(7) & 0.0069(4) & -0.369(11) \\ 0.716(4) & 0.0072(7) & 0.331(2) \\ 1.088(16) & 0.093(3) & -1.468(31) \end{pmatrix}, \qquad (11)
$$

and in the case of GeSe$_4$ the weighting factor matrix is given by

$$
\frac{\mathbf{W}'}{\mathrm{barn}} = \begin{pmatrix} 0.642(1) & 0.00007(2) & 0.034(2) \\ 0.945(8) & 0.0059(3) & -0.373(11) \\ 0.699(3) & 0.0061(6) & 0.327(2) \\ 1.16(2) & 0.079(2) & -1.518(33) \end{pmatrix}. \qquad (12)
$$

The corresponding partial pair-distribution functions are denoted by $g_{IJ}(r)$ ($I, J = \mathrm{N, C}$), and are related to the $g_{\alpha\beta}(r)$ functions via the relations

$$g_{\mathrm{NN}}(r) = c^2_{\mathrm{Ge}} g_{\mathrm{GeGe}}(r) + c^2_{\mathrm{Se}} g_{\mathrm{SeSe}}(r) + 2 c_{\mathrm{Ge}} c_{\mathrm{Se}} g_{\mathrm{GeSe}}(r), \qquad (13)$$

$$g_{\mathrm{CC}}(r) = c_{\mathrm{Ge}} c_{\mathrm{Se}} \left[g_{\mathrm{GeGe}}(r) + g_{\mathrm{SeSe}}(r) - 2 g_{\mathrm{GeSe}}(r)\right], \qquad (14)$$

$$g_{\mathrm{NC}}(r) = c_{\mathrm{Ge}} \left[g_{\mathrm{GeGe}}(r) - g_{\mathrm{GeSe}}(r)\right] - c_{\mathrm{Se}} \left[g_{\mathrm{SeSe}}(r) - g_{\mathrm{GeSe}}(r)\right]. \qquad (15)$$

Equation (9) shows that $S_{\mathrm{NN}}(k)$ would be measured directly in a diffraction experiment if $b_{\mathrm{Ge}} = b_{\mathrm{Se}}$, which is almost the case for the $^{\mathrm{nat}}\mathrm{Ge}^{\mathrm{nat}}\mathrm{Se}_3$ and $^{\mathrm{nat}}\mathrm{Ge}^{\mathrm{nat}}\mathrm{Se}_4$ samples because Ge and Se of natural isotopic abundance have very similar neutron scattering lengths. It follows that $g_{\mathrm{NN}}(r)$ will describe the sites of the scattering nuclei but cannot distinguish between the chemical species that occupy those sites, i.e., it gives information on the topological ordering. The mean coordination number $\bar{n}$ is given by

$$\bar{n} = 4\pi\rho \int_{r_1}^{r_2} \mathrm{d}r \, r^2 g_{\mathrm{NN}}(r) = c_{\mathrm{Ge}} \bar{n}_{\mathrm{Ge}} + c_{\mathrm{Se}} \bar{n}_{\mathrm{Se}}, \qquad (16)$$

where the mean coordination number of Ge atoms $\bar{n}_{\mathrm{Ge}} \equiv \bar{n}^{\mathrm{Ge}}_{\mathrm{Ge}} + \bar{n}^{\mathrm{Se}}_{\mathrm{Ge}}$ and the mean coordination number of Se atoms $\bar{n}_{\mathrm{Se}} \equiv \bar{n}^{\mathrm{Se}}_{\mathrm{Se}} + \bar{n}^{\mathrm{Ge}}_{\mathrm{Se}}$. According to the "8-N" rule, in which $\bar{n}_{\mathrm{Ge}} = 4$ and $\bar{n}_{\mathrm{Se}} = 2$, it follows that $\bar{n} = 2.5$ for GeSe$_3$ and $\bar{n} = 2.4$ for GeSe$_4$. In comparison, $S_{\mathrm{CC}}(k)$ will give information on the chemical ordering and, according to Equation (14), there will be a positive peak or negative trough in $g_{\mathrm{CC}}(r)$ if there is a preference at a given distance for like or unlike chemical species, respectively. Finally, $g_{\mathrm{NC}}(r)$ will describe the cross-correlation between sites and their occupancy by a given chemical species. A full description of the Bhatia-Thornton formalism as applied to binary network glass-forming systems is given elsewhere (Salmon, 1992, 2007b).

Equations (2) and (10) can be solved to give the full set of $S_{\alpha\beta}(k)$ or $S_{IJ}(k)$ functions by using the SVD method, which is described by Ludwig et al. (1987) and Zeidler et al. (2010). In the case of Equation (2), the two-norm condition number for the normalized weighting factor matrix is $\kappa_2' = 144$ for GeSe$_3$ vs. $\kappa_2' = 236$ for GeSe$_4$, respectively, i.e., the weighting

factor matrix for GeSe$_3$ is better conditioned (Zeidler et al., 2010). In the case of Equation (10), $\kappa'_2 = 63$ for GeSe$_3$ vs. $\kappa'_2 = 76$ for GeSe$_4$, respectively, i.e., the weighting factor matrices for the $S_{IJ}(k)$ functions are better conditioned than those for the $S_{\alpha\beta}(k)$ functions.

We note that if Equation (2) is re-written to include only the total structure factors for the nat-mix, 70-nat and 73-76 samples, then the two-norm condition number for the normalized weighting factor matrix becomes $\kappa'_2 = 133$ for GeSe$_3$ vs. $\kappa'_2 = 221$ for GeSe$_4$. The resultant $S_{\alpha\beta}(k)$ functions are in agreement with those obtained by using all four of the total structure factors and the SVD method (Rowlands, 2015). Inclusion of the total structure factor for the nat-nat sample does not improve the conditioning of the weighting factor matrix because $^{nat}_{nat}F(k)$ does not contain information on the chemical ordering in the glass: As $b_{^{nat}Ge} \simeq b_{^{nat}Se}$ it follows from Equation (9) that $^{nat}_{nat}F(k) \simeq \langle b \rangle^2 \left[S_{NN}(k) - 1 \right]$.

In practice, a diffractometer can measure over only a finite scattering vector range up to a maximum value k_{max}, which is equivalent to the multiplication of the ideal diffraction pattern by a window function $M(k)$ where $M(k \leq k_{max}) = 1$ and $M(k > k_{max}) = 0$. The Fourier transform of this window function is given by

$$M(r) = \frac{1}{\pi} \int_0^{k_{max}} dk \, \cos(kr) = \frac{k_{max}}{\pi} \text{sinc}\left(k_{max} r \right) \qquad (17)$$

where $\text{sinc}(y) \equiv \sin(y) / y$. To help in identifying those features in a measured $g_{\alpha\beta}(r)$ function that are an artifact of $M(r)$, it is convenient to consider the density function

$$d'_{\alpha\beta}(r) = \frac{2}{\pi} \int_0^\infty dk \left[S_{\alpha\beta}(k) - 1 \right] k \, M(k) \, \sin(kr)$$
$$= d_{\alpha\beta}(r) \otimes M(r), \qquad (18)$$

where $d_{\alpha\beta}(r) \equiv 4\pi\rho r \left[g_{\alpha\beta}(r) - 1 \right]$ and $\otimes$ denotes the one-dimensional convolution operator. A least-squares fit to $d'_{\alpha\beta}(r)$ can then be made by using a sum of Gaussian functions, representing the peaks in $d_{\alpha\beta}(r)$, convolved with $M(r)$ (Martin et al., 2003; Salmon and Petri, 2003). A similar procedure can also be adopted for the first-difference density functions $\Delta D'_{Ge}(r) \equiv 4\pi\rho r \left[\Delta G_{Ge}(r) / |\Delta G_{Ge}(r \rightarrow 0)| \right] \otimes M(r)$ and $\Delta D'(r) \equiv 4\pi\rho r \left[\Delta G(r) / |\Delta G(r \rightarrow 0)| \right] \otimes M(r)$. Other window functions can be used to reduce the severity of Fourier transform artifacts.

3. EXPERIMENTAL

3.1. Synthesis and Characterization of Glassy GeSe$_3$ and GeSe$_4$

The Ge isotopes used for the sample preparation were processed in order to remove oxide impurities. Finely powdered isotope was loaded into a glass crucible, with a fritted glass bottom of 3 μm pore size, and placed within a reduction furnace. The furnace was flushed with Ar gas to remove air, and the gas flow was switched to hydrogen. Next, the furnace temperature was increased to 873 K at a rate of 4 K min^{-1}, left for 48 h, and reduced to ambient

at a rate of 1 K min^{-1}. The gas flow was then switched back to Ar. This procedure gave a yield of ~83% and delivered Ge powder that had changed in appearance from black to metallic grey. Infra-red transmission spectroscopy experiments on the powder showed no indication of the Ge-O absorption band at ~879 cm^{-1} (Madon et al., 1991; Micoulaut et al., 2006), consistent with test experiments in which the reduction procedure was used to remove the oxygen from crystalline GeO$_2$, or the oxygen impurities from crystalline Ge.

Two diffraction experiments were performed, the first on glassy GeSe$_4$ and the second on glassy GeSe$_3$. Each GeSe$_4$ sample was prepared by loading elemental ^{nat}Ge (99.999%, Alfa Aesar), ^{70}Ge (95.30% ^{70}Ge, 4.10% ^{72}Ge, 0.51 % ^{76}Ge, 0.05% ^{74}Ge and 0.04% ^{73}Ge, Isoflex USA), or ^{73}Ge (95.60% ^{73}Ge, 2.34% ^{72}Ge, 2.03% ^{74}Ge, 0.025% ^{70}Ge and 0.005% ^{76}Ge, Isoflex USA) together with ^{nat}Se (99.999+%, Sigma Aldrich), ^{76}Se (99.8 % ^{76}Se and 0.20 % ^{77}Se, Isoflex USA), or ^{mix}Se (a 49.5:50.5 mixture by mass of ^{nat}Se and ^{76}Se) in the required mass ratio into a silica ampoule within a high-purity argon-filled glove box. The ampoule, of 5 mm inner diameter and 1 mm wall thickness, had previously been etched using a 48 wt% solution of hydrofluoric acid, rinsed using water then acetone, and baked dry under vacuum at 1073 K for 2 h. Once loaded, the ampoule was isolated using a Young's tap, and transferred to a vacuum line where it was sealed under a pressure of 10^{-5} Torr. The sealed ampoule was placed in a furnace that was rocked at a rate of 0.57 rpm with a maximum rocking angle of 30° to the horizontal. The furnace was heated at a rate of 1 K min^{-1} from ambient to a temperature $T = 1{,}248$ K, dwelling for 4 h each at $T = 494$ K, $T = 958$ K, and $T = 1{,}211$ K, near to the melting and boiling points of Se and the melting point of Ge, respectively. The highest temperature was maintained for 48 h before the rocking motion was stopped, the furnace was placed vertically and left for 4 h, and the furnace was then cooled at a rate of 1 K min^{-1} to $T = 928$ K (~100 K above the melting point of GeSe$_4$) where the sample was left to equilibrate for 4 h. The ampoule was then dropped into an ice/water mixture. The glassy samples separated cleanly from the their silica ampoules, which were broken open in a high-purity argon-filled glove box. The GeSe$_3$ samples were prepared from the GeSe$_4$ samples by adding elemental Ge of matched isotopic abundance, quenching from 1,027 K, and otherwise following the same method. The mass of the prepared samples was ~1.5–2.2 g, and the precise sample stoichiometry, as determined by mass, was 0.2496(3) Ge: 0.7504(3) Se for GeSe$_3$ vs. 0.1998(3) Ge: 0.8002(3) Se for GeSe$_4$.

The measured infrared transmission spectra for the GeSe$_3$ and GeSe$_4$ glasses showed no indication of Ge-O or Se-O impurity bands, e.g., in the region around 735–781 cm^{-1} (Savage and Nielsen, 1965). A similarly prepared sample of GeSe$_4$ glass, but with only 12 h of rocking, was characterized using energy dispersive X-ray spectroscopy and Raman spectroscopy, and was found to be homogeneous on a sub-micron to centimeter length scale (Lucas et al., 2019). The mass density, as measured using a helium pycnometer, was 4.309(3) g cm^{-3} or 4.334(4) g cm^{-3} for the GeSe$_3$ and GeSe$_4$ glasses, respectively, corresponding to an atomic number density of $\rho = 0.03353(2)$ Å^{-3} or $\rho = 0.03359(3)$ Å^{-3}, respectively. A single glass transition temperature of $T_g = 523(3)$ K for GeSe$_3$ or $T_g = 463(3)$ K for

GeSe$_4$ was measured by using modulated differential scanning calorimetry with a scan rate of 3 K min^{-1} and modulation of 1 K per 100 s.

3.2. Neutron Diffraction Experiments

The diffraction experiments were performed using the D4c instrument at the Institut Laue-Langevin (Fischer et al., 2002). The Cu(220) reflections from a monochromator gave an incident neutron wavelength $\lambda = 0.4990(1)$ Å, and the $\lambda/2$ reflections were suppressed by using a Rh filter. The monochromator crystals were orientated to focus the neutron beam in both the horizontal and vertical directions, thus maximizing the flux of neutrons at the sample position. The same cylindrical vanadium container, of inner diameter 4.8 mm and wall thickness 0.1 mm, was used for each set of experiments to ensure a reproducible scattering geometry. The samples were loaded into the container within a high-purity argon-filled glove box. Diffraction patterns were measured at room temperature ($\simeq$298 K) for each of the samples in its container, the empty container, the empty instrument, and a cylindrical vanadium rod of diameter 6.08 mm for normalization purposes. The diffraction pattern was also measured for a slab of neutron absorbing ^{10}B$_4$C of dimensions similar to the sample in order to estimate the effect of the sample's attenuation on the background count-rate at small scattering angles (Bertagnolli et al., 1976). The relative counting times for the sample-in-container and empty container measurements were optimized in order to minimize the statistical error on the container-corrected intensity (Salmon et al., 2016). The counting times for each of the sample-in-container measurements was ~18 h for the GeSe$_3$ experiment vs. ~22 h for the GeSe$_4$ experiment. The count-rate stability was checked by saving the measured intensity for a given setup at regular intervals, and a comparison between these intensities showed no deviation within the statistical error. The count-rate stability of the D4c instrument is measured to be $\pm$0.012(8)% (Zeidler et al., 2012).

The total structure factors were obtained by following the data analysis procedure described by Salmon et al. (1998), and self-consistency checks were made to assess the reliability of the measured functions. For instance, it is necessary that (i) the measured intensities are greater than or equal to zero which leads to the condition $S_{NN}(k)S_{CC}(k) \geq S_{NC}(k)^2$; (ii) each of the Faber-Ziman partial structure factors satisfies the sum-rule relation $\int_0^\infty dk\, k^2 \left[S_{\alpha\beta}(k) - 1\right] = -2\pi^2\rho$ as found by taking the low-r limit of Equation (5); (iii) the measured $g_{\alpha\beta}(r)$ functions oscillate about zero at r-values smaller than the distance of closest approach between two atoms; and (iv) when these oscillations in $g_{\alpha\beta}(r)$ are set to zero, the back Fourier transform should be in good overall agreement with the original partial structure factor.

4. RESULTS

There is significant contrast between the total structure factors $F(k)$ measured for the different isotopically enriched samples of glassy GeSe$_3$ or GeSe$_4$ (**Figure 1**). A so-called first sharp diffraction peak is observable at $k_{FSDP} = 1.06(1)$ Å^{-1} for GeSe$_3$ vs. $k_{FSDP} = 1.12(2)$ Å^{-1} for GeSe$_4$, and is a signature of ordering on an intermediate length scale (Salmon, 1994). As
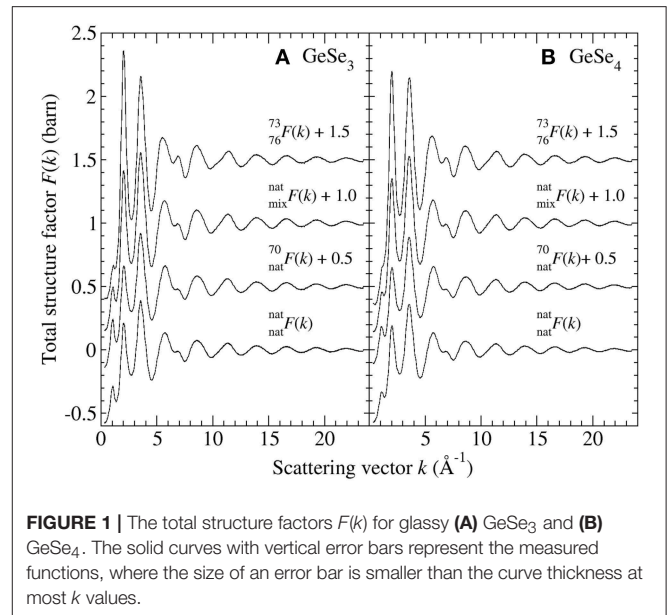

FIGURE 1 | The total structure factors $F(k)$ for glassy **(A)** GeSe$_3$ and **(B)** GeSe$_4$. The solid curves with vertical error bars represent the measured functions, where the size of an error bar is smaller than the curve thickness at most k values.

shown in **Figure 2**, the FSDP appears as a peak in $\Delta F_{Ge}(k)$, for which the Ge-Ge and Ge-Se partial structure factors receive positive weighting factors [Equation (7)], and as a trough in $\Delta F(k)$, for which the Ge-Ge and Se-Se partial structure factors receive negative and positive weighting factors, respectively [Equation (8)]. These observations are consistent with the FSDP having contributions from both $S_{GeGe}(k)$ and $S_{GeSe}(k)$.

Figure 3 shows the $\Delta D'_{Ge}(r)$ and $\Delta D'(r)$ functions for glassy GeSe$_3$ and GeSe$_4$, obtained by Fourier transforming the spline-fitted reciprocal-space functions shown in **Figure 2** with $k_{max} = 23.5$ Å^{-1}. The first peaks in $\Delta D'_{Ge}(r)$ and $\Delta D'(r)$ were assumed to have contributions solely from Ge-Se and Se-Se nearest-neighbors, respectively, i.e., homonuclear Ge-Ge bonds were assumed to be rare. The first peak in each function was then fitted to a single Gaussian function convoluted with the modification function $M(r)$. In the case of GeSe$_3$, the fits gave a Ge-Se nearest-neighbor distance $\bar{r}_{GeSe} = 2.37(2)$ Å with $\bar{n}^{Se}_{Ge} = 4.02(2)$ and a Se-Se nearest-neighbor distance $\bar{r}_{SeSe} = 2.35(2)$ Å with $\bar{n}^{Se}_{Se} = 0.72(2)$, corresponding to a goodness-of-fit parameter R_χ (Wright, 1993) of 0.055 or 0.048, respectively, for a fitted range of 1.5–3.0 Å. In the case of GeSe$_4$, the fits gave $\bar{r}_{GeSe} = 2.37(2)$ Å with $\bar{n}^{Se}_{Ge} = 4.02(5)$ and $\bar{r}_{SeSe} = 2.35(2)$ Å with $\bar{n}^{Se}_{Se} = 1.01(2)$, corresponding to an R_χ value of 0.022 or 0.044, respectively, for a fitted range of 1.5–3.0 Å.

Figure 4 shows the full set of partial structure factors $S_{\alpha\beta}(k)$ for glassy GeSe$_3$, as extracted from the total structure factors shown in **Figure 1A** by using the SVD method. The results show that $S_{GeGe}(k)$ has the most prominent FSDP at $k_{FSDP} = 1.01(1)$ Å^{-1}, and that $S_{GeSe}(k)$ also has a small FSDP at $k_{FSDP} = 1.11(1)$ Å^{-1}. The density functions $d'_{\alpha\beta}(r)$ of **Figure 5A** were obtained by Fourier transforming the spline fitted $S_{\alpha\beta}(k)$ functions of **Figure 4** with $k_{max} = 23.5$ Å^{-1}, where a Lorch window function (Lorch, 1969; Salmon, 2006) was also applied to $S_{GeGe}(k)$ in order to reduce Fourier transform artifacts. The

first peak in $d'_{GeSe}(r)$ and $d'_{SeSe}(r)$ was fitted to a single Gaussian function convoluted with $M(r)$. The fits gave $\bar{r}_{GeSe} = 2.37(2)$ Å with $\bar{n}^{Se}_{Ge} = 4.00(2)$ and $\bar{r}_{SeSe} = 2.35(2)$ Å with $\bar{n}^{Se}_{Se} = 0.70(2)$, corresponding to an R_χ value of 0.048 or 0.047, respectively, for a fitted range of 1.5–3.0 Å. These values are consistent with
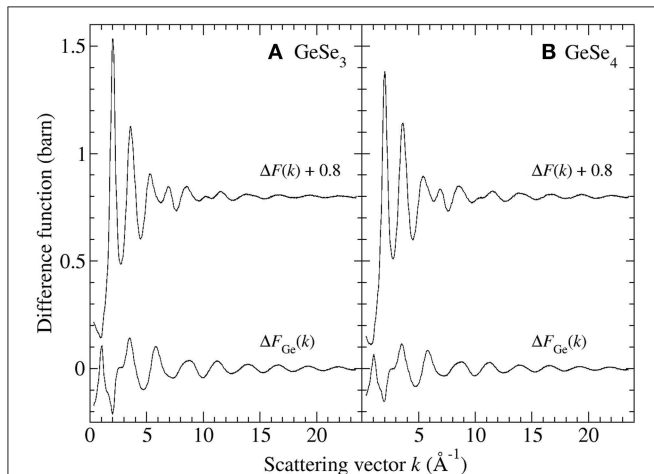
those obtained from the first-difference functions, and point to a network structure that is built from Ge(Se$_4$)$_{1/2}$ tetrahedra and Se$_n$ chains (n is an integer ≥ 2) where the homonuclear Se-Se bond distance is 2.35(2) Å. The peak in $d'_{GeGe}(r)$ at 2.70(2) Å has a position that is larger than expected for homonuclear Ge-Ge bond distances of 2.33–2.42 Å (Salmon, 2007a), and it was therefore discounted as a real feature. In the structure of high-temperature crystalline GeSe$_2$, the Ge-Ge distances for edge-sharing (ES) and corner-sharing (CS) Ge(Se$_4$)$_{1/2}$ tetrahedra are 3.05 and 3.51–3.60 Å, respectively (Dittmar and Schäfer, 1976). The peaks in $d'_{GeGe}(r)$ at 3.04(3) and 3.58(2) Å were therefore assigned to the Ge-Ge distances for ES and CS Ge(Se$_4$)$_{1/2}$ tetrahedra, respectively.

Figure 6 shows the full set of partial structure factors $S_{\alpha\beta}(k)$ for glassy GeSe$_4$, as extracted from the total structure factors shown in **Figure 1B** by using the SVD method. The results show that $S_{GeGe}(k)$ has the most prominent FSDP at $k_{FSDP} = 0.97(2)$ Å^{-1}, and that $S_{GeSe}(k)$ also has a small FSDP at $k_{FSDP} = 1.08(2)$ Å^{-1}. The density functions $d'_{\alpha\beta}(r)$ of **Figure 5B** were obtained by Fourier transforming the spline fitted $S_{\alpha\beta}(k)$ functions of **Figure 6** with $k_{max} = 23.5$ Å^{-1}, where a cosine window function was also applied to $S_{GeGe}(k)$ over the range $21.45 \leq k$ (Å^{-1}) ≤ 23.5 in order to reduce Fourier transform artifacts. The first peak in $d'_{GeSe}(r)$ and $d'_{SeSe}(r)$ was fitted to a single Gaussian function convoluted with $M(r)$. The fits gave $\bar{r}_{GeSe} = 2.37(2)$ Å with $\bar{n}^{Se}_{Ge} = 4.04(5)$ and $\bar{r}_{SeSe} = 2.35(2)$ Å with $\bar{n}^{Se}_{Se} = 1.00(2)$, corresponding to an R_χ value of 0.055

FIGURE 2 | The first-difference functions $\Delta F_{Ge}(k)$ and $\Delta F(k)$ for glassy **(A)** GeSe$_3$ and **(B)** GeSe$_4$. The solid curves with vertical error bars represent the measured functions, where the size of an error bar is smaller than the curve thickness at most k values.
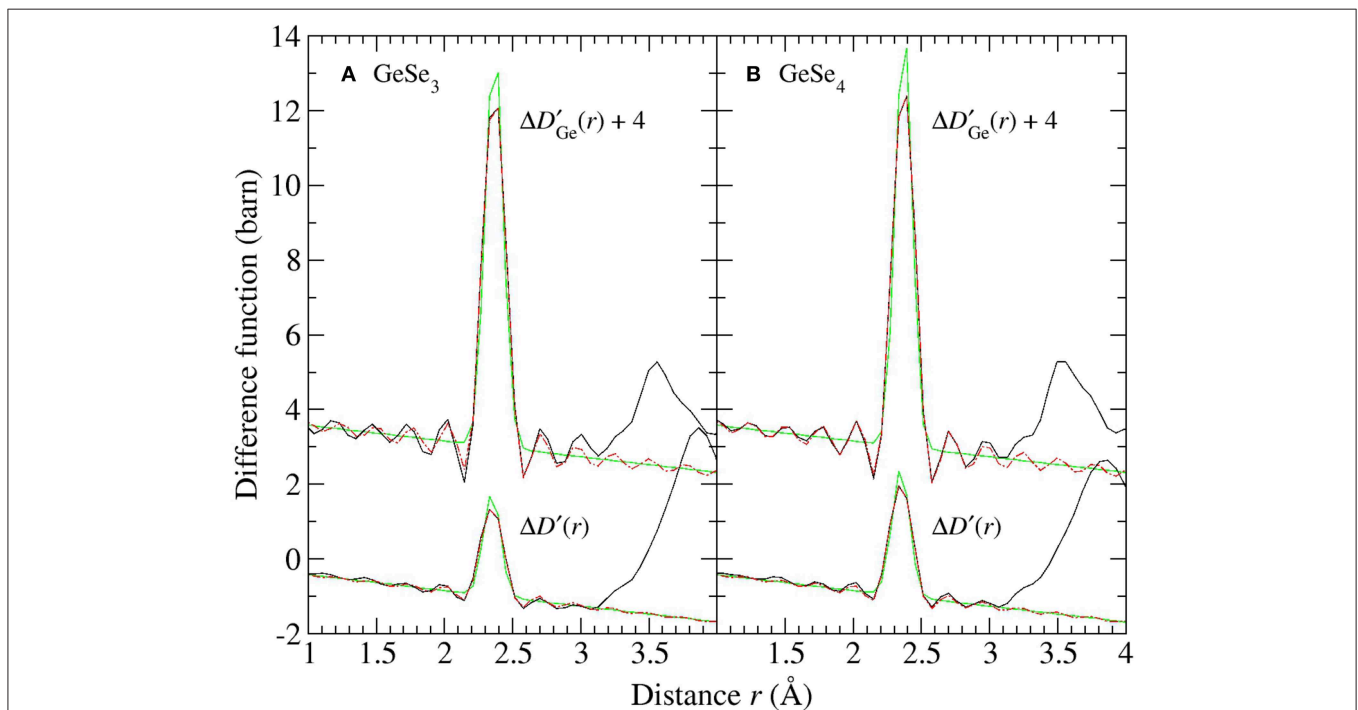
FIGURE 3 | The first-difference density functions $\Delta D'_{Ge}(r)$ and $\Delta D'(r)$ for glassy **(A)** GeSe$_3$ and **(B)** GeSe$_4$ where the solid (black) curves were obtained by spline-fitting and Fourier transforming the $\Delta F_{Ge}(k)$ and $\Delta F(k)$ functions shown in **Figure 2**. In each case, the chained (red) curve shows a fit of the first peak in the measured function to a single Gaussian function [light solid (green) curve] convoluted with $M(r)$.
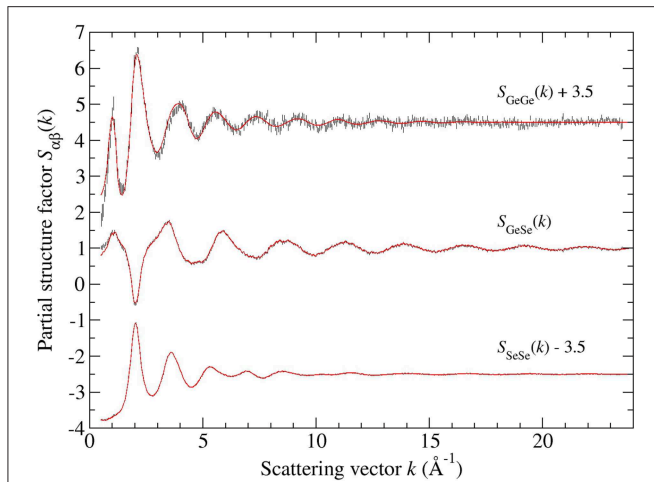
FIGURE 4 | The Faber-Ziman partial structure factors $S_{\alpha\beta}(k)$ for glassy $GeSe_3$, obtained from the measured total structure factors of **Figure 1A** by using the SVD method. The vertical error bars represent the measured data points with statistical errors. The solid (red) curves are the back Fourier transforms of the corresponding partial pair-distribution functions $g_{\alpha\beta}(r)$ given by the solid curves in **Figure 7**.

FIGURE 6 | The Faber-Ziman partial structure factors $S_{\alpha\beta}(k)$ for glassy $GeSe_4$, obtained from the measured total structure factors of **Figure 1B** by using the SVD method. The vertical error bars represent the measured data points with statistical errors. The solid (red) curves are the back Fourier transforms of the corresponding partial pair-distribution functions $g_{\alpha\beta}(r)$ given by the solid curves in **Figure 8**.

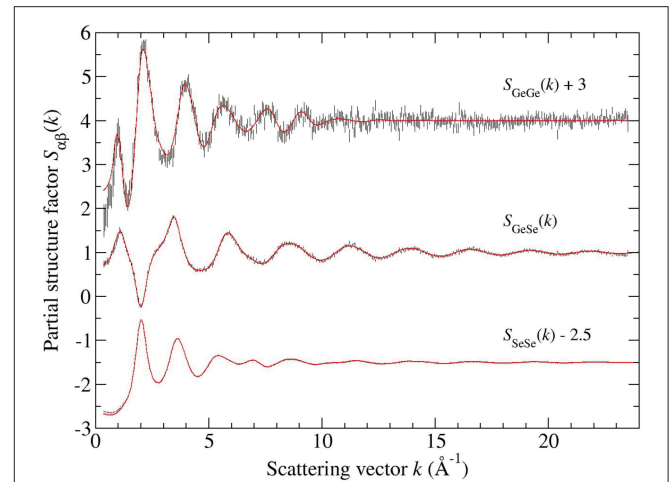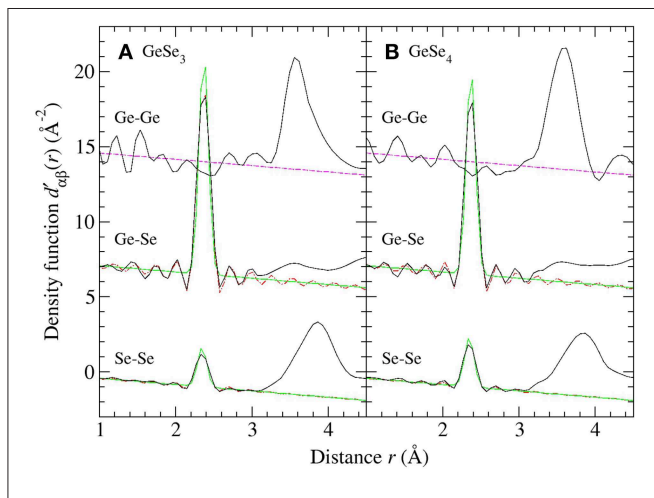**FIGURE 5 |** The density functions $d'_{\alpha\beta}(r)$ for glassy **(A)** $GeSe_3$ and **(B)** $GeSe_4$ where the solid (black) curves were obtained by Fourier transforming the spline-fitted $S_{\alpha\beta}(k)$ functions shown in **Figures 4**, **6**, respectively. For $d'_{GeGe}(r)$, the broken (magenta) line gives the locus of points for which $d'_{GeGe}(r) = -4\pi\rho r$. For $d'_{GeSe}(r)$ and $d'_{SeSe}(r)$, the chained (red) curve shows a fit of the first peak to a single Gaussian function [light solid (green) curve] convoluted with $M(r)$. The Ge-Se and Ge-Ge data sets have been shifted vertically for clarity of presentation.

FIGURE 7 | The partial pair-distribution functions $g_{\alpha\beta}(r)$ for glassy $GeSe_3$ after the effect of $M(r)$ has been removed.

or 0.052, respectively, for a fitted range of 1.5–3.0 Å. These values are consistent with those obtained from the first-difference functions, and point to a network structure that is built from $Ge(Se_4)_{1/2}$ tetrahedra and Se_n chains. The $d'_{GeGe}(r)$ function shows no evidence of homonuclear Ge-Ge bonds, and does not display a peak at $\simeq 3.04$ Å that can be assigned to ES $Ge(Se_4)_{1/2}$ tetrahedra. The first peak at 3.59(1) Å is, however, broader than the corresponding feature for $GeSe_3$, with a low-r cutoff of 3.07(3) Å that is typical of ES tetrahedral distances.

The final Ge-Se and Se-Se $d_{\alpha\beta}(r)$ functions were obtained by merging smoothly the Gaussian representation of $d_{GeSe}(r)$ or $d_{SeSe}(r)$ in the first-peak region, where the effect of $M(r)$ on $d'_{GeSe}(r)$ and $d'_{SeSe}(r)$ is measurable, with the $d'_{\alpha\beta}(r)$ functions at higher-r values. The $d'_{GeSe}(r)$ function at these higher-r values was smoothed by the application of a Lorch window function. In comparison, $d_{GeGe}(r)$ was set equal to the measured $d'_{GeGe}(r)$ function at all r values. In each case, the unphysical oscillations at r values less than the distance of closest approach between the centers of two atoms were set to $d_{\alpha\beta}(r) = -4\pi\rho r$. The final $d_{\alpha\beta}(r)$ functions were then converted to the $g_{\alpha\beta}(r)$ functions shown in **Figures 7**, **8** for glassy $GeSe_3$ and $GeSe_4$, respectively. The back Fourier transforms of these $g_{\alpha\beta}(r)$ functions are
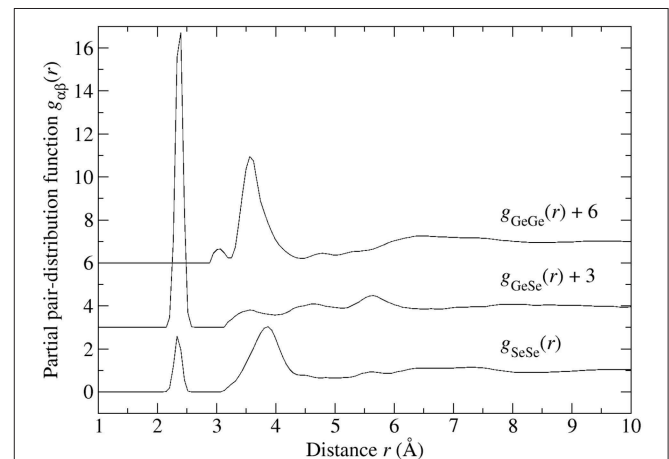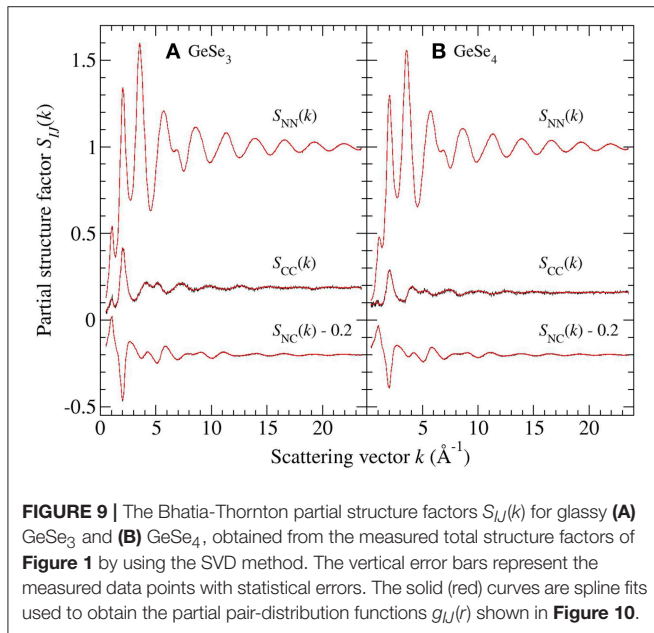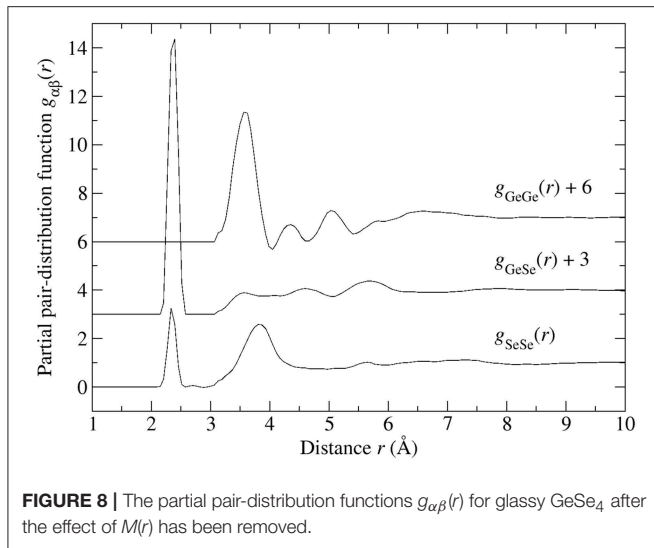
FIGURE 8 | The partial pair-distribution functions $g_{\alpha\beta}(r)$ for glassy GeSe$_4$ after the effect of $M(r)$ has been removed.

FIGURE 9 | The Bhatia-Thornton partial structure factors $S_{IJ}(k)$ for glassy **(A)** GeSe$_3$ and **(B)** GeSe$_4$, obtained from the measured total structure factors of **Figure 1** by using the SVD method. The vertical error bars represent the measured data points with statistical errors. The solid (red) curves are spline fits used to obtain the partial pair-distribution functions $g_{IJ}(r)$ shown in **Figure 10**.

FIGURE 10 | The Bhatia-Thornton partial pair-distribution functions $g_{IJ}(r)$ for glassy **(A)** GeSe$_3$ and **(B)** GeSe$_4$. The solid black curves were obtained by Fourier transforming the spline fitted partial structure factors shown in **Figure 9** and setting the unphysical oscillations at r values smaller than the distance of closest approach between the centers of two atoms [broken (red) curves] to the $g_{IJ}(r \rightarrow 0)$ limit. The insets show the larger-r features in $rg_{CC}(r)$, and the arrowed lines indicate the periodicity expected from the position of the principal peak in $S_{CC}(k)$ at $k_{PP} \simeq 2.03$ Å^{-1}.

compared to the measured partial structure factors for glassy GeSe$_3$ and GeSe$_4$ in **Figures 4**, **6**, respectively.

The Bhatia-Thornton partial structure factors $S_{IJ}(k)$ and corresponding partial pair-distribution functions $g_{IJ}(r)$ are shown in **Figures 9**, **10**, respectively. As discussed in section 2, the weighting factor matrix used to obtain the $S_{IJ}(k)$ functions is better conditioned than the matrix used to obtain the $S_{\alpha\beta}(k)$ functions, which accounts for the reduction in size of the error bars for $S_{CC}(k)$ as compared to $S_{GeGe}(k)$. For each material, the inequality relation $S_{NN}(k)S_{CC}(k) \geq S_{NC}(k)^2$ is fulfilled within the statistical error at all k values (section 3.2). Each set of partial structure factors shows an FSDP in the range 1.01(2)–1.05(2) Å^{-1} for GeSe$_3$ vs. 0.91(2)–1.11(2) Å^{-1} for GeSe$_4$, and a principal peak or trough in the range 2.01(2)–2.04(2) Å^{-1} for GeSe$_3$ vs. 1.99(2)–2.03(2) Å^{-1} for GeSe$_4$.
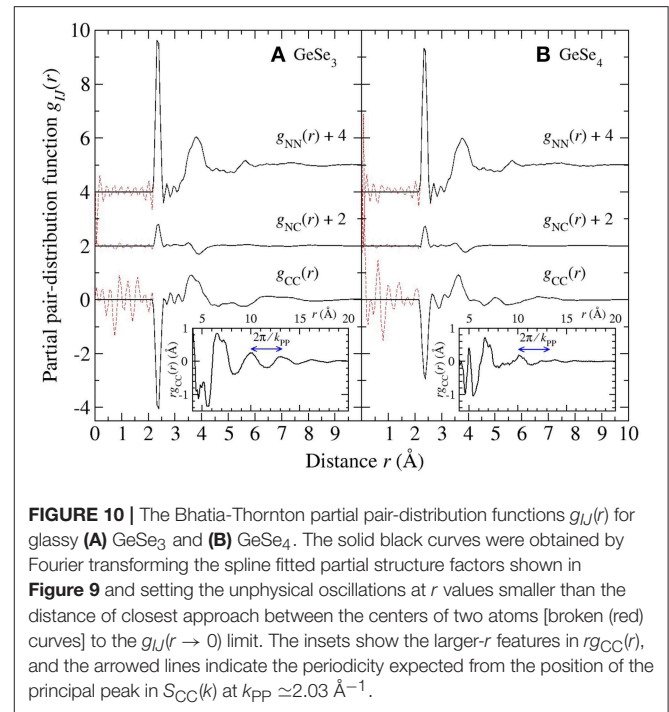
As in the case of glassy GeSe$_2$, the FSDP in $S_{CC}(k)$ for glassy GeSe$_3$ and GeSe$_4$ indicates the presence of concentration fluctuations on an intermediate length scale (Penfold and Salmon, 1991; Salmon, 1992). This feature arises from the Ge-Ge and Ge-Se pair-correlation functions, in keeping with the relation

$$S_{CC}(k) = c_{Ge}c_{Se}\{1 + c_{Ge}c_{Se}\left[S_{GeGe}(k) + S_{SeSe}(k) - 2S_{GeSe}(k)\right]\}$$
(19)

and the measured $S_{\alpha\beta}(k)$ functions shown in **Figures 4**, **6**. From the properties of Fourier transforms, a sharp peak in $S_{CC}(k)$ at k_i is associated with real-space ordering of periodicity $2\pi/k_i$ that decays with a correlation length of $2\pi/\Delta k_i$, where Δk_i is the peak width (Salmon, 1994). The most prominent feature in $S_{CC}(k)$ is the principal peak at $k_{PP} \simeq 2.03$ Å^{-1} with a height that decreases in the order from GeSe$_2$ to GeSe$_3$ to GeSe$_4$. The Fourier transform of $S_{CC}(k)$ shows oscillations of periodicity $2\pi/k_{PP}$ that are readily discernable for GeSe$_2$ (Salmon, 2006) and GeSe$_3$ (inset to **Figure 10A**). Similarly, the small FSDP in $S_{CC}(k)$ at k_{FSDP} will originate from a real-space length scale that is commensurate with $2\pi/k_{FSDP}$, i.e., the Ge atoms in the network structures are not distributed uniformly on an intermediate length scale. In the context of FPMD simulations, the appearance of this FSDP is significant because its reproduction has necessitated the use of exchange and correlation energy functionals that enhance charge transfer between the Ge and Se atoms (Massobrio et al., 1999, 2000, 2010; Micoulaut et al., 2009, 2013).

5. DISCUSSION
5.1. Network Structure

The measured Ge-Se coordination numbers for glassy GeSe$_2$ (Petri et al., 2000; Salmon and Petri, 2003), GeSe$_3$ and GeSe$_4$

indicate the formation of $Ge(Se_4)_{1/2}$ tetrahedra (**Table 1**). The Ge-Se:Se-Se distance ratio, obtained from the nearest-neighbor Ge-Se and next-nearest-neighbor Se-Se peak positions, is 0.607(6), 0.616(6), or 0.619(6) for $GeSe_2$, $GeSe_3$, and $GeSe_4$, respectively, and the intra-tetrahedral Se-Ge-Se bond angle obtained from these peak positions is 111(1)°, 109(1)°, or 108(1)°, respectively. In comparison, for a regular tetrahedron, the Ge-Se:Se-Se distance ratio is $\sqrt{3/8} = 0.612$, and the intra-tetrahedral Se-Ge-Se bond angle is 109.47°. The Ge-Se-Se bond angle, estimated from the first and second peak positions in $g_{GeSe}(r)$, is 98(2)° for both $GeSe_3$ and $GeSe_4$.

For all of the glasses, the peak in $g_{SeSe}(r)$ at $\bar{r}_{SeSe} \simeq 2.34$ Å originates from homonuclear Se-Se bonds, and the corresponding coordination number increases with the Se content of the glass. A comparison of the $\bar{n}_{Se}^{Se}$ values with those found from ^{77}Se NMR experiments (Gjersing et al., 2010b; Kaseman et al., 2016) is given in **Table 2**. Here, the NMR experiments provide the fractions of Se atoms in Se-Se-Se vs. Ge-Se-Se connections, and the corresponding Se-Se coordination numbers follow from $\bar{n}_{Se}^{Se}(Se\text{-}Se\text{-}Se) = (N_{Se,Se\text{-}Se\text{-}Se} / N_{Se}) \times 2$ and $\bar{n}_{Se}^{Se}(Ge\text{-}Se\text{-}Se) = (N_{Se,Ge\text{-}Se\text{-}Se} / N_{Se}) \times 1$, where $N_{Se,Se\text{-}Se\text{-}Se}$ is the number of Se atoms bound to two other Se atoms in a Se-Se-Se connection, $N_{Se,Ge\text{-}Se\text{-}Se}$ is the number of Se atoms bound to one Ge atom and one Se atom in a Ge-Se-Se connection, and N_{Se} is the total number of Se atoms in the glass.

For $GeSe_2$, the peak in $g_{GeGe}(r)$ at $\bar{r}_{GeGe} = 2.42(2)$ Å originates from homonuclear Ge-Ge bonds, but there is no evidence of these bonds in either $GeSe_3$ or $GeSe_4$. For $GeSe_2$ and $GeSe_3$, the peak in $g_{GeGe}(r)$ at $\bar{r}_{GeGe} \simeq 3.02$–$3.04$ Å originates from ES $Ge(Se_4)_{1/2}$ tetrahedra, but this feature is absent for $GeSe_4$. The associated inter-tetrahedral Ge-Se-Ge bond angle, estimated from the nearest-neighbor Ge-Se and ES Ge-Ge distances, is 80(1)°.

For all of the glasses, the peak in $g_{GeGe}(r)$ at $\bar{r}_{GeGe} \simeq 3.57$ Å will have a contribution from CS $Ge(Se_4)_{1/2}$ tetrahedra (Petri

et al., 2000; Salmon and Petri, 2003), and the associated inter-tetrahedral Ge-Se-Ge bond angle, estimated from the nearest-neighbor Ge-Se and CS Ge-Ge distances, is 98(2)°. In comparison, for the high-temperature crystalline phase of $GeSe_2$ (Dittmar and Schäfer, 1976), the Ge-Se-Ge bond angle is in the range of 80.2–80.6° for ES tetrahedra vs. 96.2–100.1° for CS tetrahedra.

For $GeSe_3$ and $GeSe_4$, there will be contributions to $g_{GeGe}(r)$ from the Ge-Ge distances within Ge-Se_n-Ge connections. For instance, in the case of $GeSe_4$ there are peaks at 4.34(2) Å and 5.06(2) Å that do not appear to be Fourier transform artifacts, with coordination numbers of $\bar{n}_{Ge}^{Ge} = 0.33(2)$ and $\bar{n}_{Ge}^{Ge} = 1.28(2)$, respectively. If these peaks originate from Ge-Se-Se-Ge connections, then the associated Ge-Ge distance will depend on the relative rotation of these Ge atoms about the Se-Se bond, i.e., on the dihedral angle ϕ between two planes that contain both of the Se atoms and either the first or the second Ge atom in a Ge-Se-Se-Ge connection. For a Ge-Se-Se bond angle of 98° and bond distances of $\bar{r}_{GeSe} = 2.37$ Å and $\bar{r}_{SeSe} = 2.35$ Å, a Ge-Ge distance of 4.34 Å is obtained for $\phi \simeq 84°$, and a Ge-Ge distance of 5.06 Å is obtained for $\phi \simeq 120°$.

For each glass, the NDIS experiments give $\bar{n}_{Ge} = 4$ and $\bar{n}_{Se} = 2$ within the experimental error (**Table 2**), and the overall mean coordination numbers $\bar{n}$ are in agreement with those obtained from the first peak in the $g_{NN}(r)$ functions of **Figure 10** [see Equation (16)]. The NDIS results are therefore consistent with the expectations of the "8-N" rule (Zeidler et al., 2017). In comparison, the fraction of Se atoms in Ge-Se-Ge connections has been measured for several Ge_xSe_{1-x} glasses with $x \leq 1/3$ by using ^{77}Se NMR spectroscopy (Gjersing et al., 2010b; Kaseman et al., 2016). The Se-Ge coordination numbers for CS and ES connections are given by the expressions $\bar{n}_{Se}^{Ge}(CS) = (N_{Se,CS} / N_{Se}) \times 2$ and $\bar{n}_{Se}^{Ge}(ES) = (N_{Se,ES} / N_{Se}) \times 2$, respectively, where $N_{Se,CS}$ and $N_{Se,ES}$ are the numbers of Se atoms in CS and ES connections, respectively. The $\bar{n}_{Se}^{Ge}$ values extracted from the ^{77}Se NMR results for glassy $GeSe_2$ and $GeSe_4$ are compared to the NDIS results in **Table 2**. Both techniques give a mean coordination number $\bar{n}_{Se} = \bar{n}_{Se}^{Se} + \bar{n}_{Se}^{Ge} = 2$, although there is a discrepancy for $GeSe_4$ between the relative contributions to $\bar{n}_{Se}$ from $\bar{n}_{Se}^{Se}$ vs. $\bar{n}_{Se}^{Ge}$. A similar set of findings was obtained by re-interpreting the measured ^{77}Se MAS NMR spectra for glassy $GeSe_2$ and $GeSe_4$ (Gjersing et al., 2010b) by using the isotropic chemical shifts calculated for the ^{77}Se nucleus via density-functional-theory based NMR calculations for amorphous model structures generated by FPMD (Kibalchenko et al., 2011) (**Table 2**). The associated Ge-Se coordination numbers are given by $\bar{n}_{Ge}^{Se} = (c_{Se} / c_{Ge}) \bar{n}_{Se}^{Ge} = [(1 - x) / x] \bar{n}_{Se}^{Ge}$, and are also shown in **Table 2**. For the case of $GeSe_4$, the $\bar{n}_{Ge}^{Se}$ values extracted from the ^{77}Se NMR results are larger than expected from the "8-N" rule.

Within the framework of the "8-N" rule, the chemically ordered network (CON) and random covalent network (RCN) models provide simple but contrasting viewpoints of the network structures (Salmon, 2007a). In the CON, Ge-Se bonds are favored. It follows that only Ge-Se and Se-Se bonds are allowed for compositions with $x < 1/3$ such that $\bar{n}_{Ge}^{Se} = 4$, $\bar{n}_{Se}^{Se} = $

TABLE 1 | The positions $\bar{r}_{\alpha\beta}$ and coordination numbers $\bar{n}_{\alpha}^{\beta}$ found from the first few peaks in the partial pair-distribution functions $g_{\alpha\beta}(r)$ measured by NDIS in the work of Petri et al. (2000) and Salmon and Petri (2003) for glassy $GeSe_2$, and in the present work for glassy $GeSe_3$ and $GeSe_4$.

Glass	α–β	$\bar{r}_{\alpha\beta}$ (Å)	$\bar{n}_{\alpha}^{\beta}$	$\bar{r}_{\alpha\beta}$ (Å)	$\bar{n}_{\alpha}^{\beta}$	$\bar{r}_{\alpha\beta}$ (Å)	$\bar{n}_{\alpha}^{\beta}$
$GeSe_2$	Ge–Ge	2.42(2)	0.25(5)	3.02(2)	0.34(5)	3.57(2)	3.2(3)
	Ge–Se	2.36(2)	3.7(1)				
	Se–Se	2.32(2)	0.20(5)	3.89(2)	9.3(2)		
$GeSe_3$	Ge–Ge	–	–	3.04(3)	0.16(5)	3.57(2)	3.2(1)
	Ge–Se	2.37(2)	4.00(2)	3.57(3)			
	Se–Se	2.34(2)	0.70(2)	3.85(2)	9.2(2)		
$GeSe_4$	Ge–Ge	–	–	–	–	3.58(2)	2.5(2)
	Ge–Se	2.37(2)	4.04(5)	3.57(2)			
	Se–Se	2.35(2)	1.00(2)	3.83(2)	9.0(2)		

The coordination numbers were obtained from Equation (6) with r_1 set at the position of the minimum on the low-r side of a given peak in $g_{\alpha\beta}(r)$, and r_2 set at the position of either the minimum or shoulder on the high-r side of that peak.

TABLE 2 | The composition dependence of the nearest-neighbor coordination numbers.

Glass	Origin	$\bar{n}_{Ge}^{Se}$	$\bar{n}_{Ge}^{Ge}$	$\bar{n}_{Ge}$	$\bar{n}_{Se}^{Ge}$	$\bar{n}_{Se}^{Se}$	$\bar{n}_{Se}$	$\bar{n}$
GeSe$_2$	NDIS[a]	3.7(1)	0.25(5)	3.95(11)	1.85(5)	0.20(5)	2.05(7)	2.68(6)
	^{77}Se NMR[b]	3.68(13)	–	–	1.84(6)	0.160(8)	2.00(6)	–
	FPMD/^{77}Se NMR[c]	3.6	–	–	1.8	0.2	2	–
	FPMD[d]	3.55	0.25	3.80	1.77	0.3	2.07	2.65
	FPMD[e]	3.65	0.29	3.94	1.82	0.2	2.02	2.66
	CON	4	0	4	2	0	2	8/3 = 2.67
	RCN	2	2	4	1	1	2	8/3 = 2.67
GeSe$_3$	NDIS[f]	4.00(2)	0	4.00(2)	1.333(7)	0.70(2)	2.03(2)	2.52(3)
	FPMD[d]	3.87	0.13	4.00	1.29	0.71	2.00	2.5
	CON	4	0	4	4/3 = 1.333	2/3 = 0.667	2	2.5
	RCN	2.4	1.6	4	0.8	1.2	2	2.5
GeSe$_4$	NDIS[f]	4.04(5)	0	4.04(5)	1.01(1)	1.00(2)	2.01(2)	2.42(2)
	^{77}Se NMR[b]	4.32(15)	–	–	1.08(4)	0.90(2)	1.98(4)	–
	^{77}Se NMR[g]	4.37(19)	–	–	1.09(4)	0.91(2)	2.00(5)	–
	FPMD/^{77}Se NMR[c]	4.52	–	–	1.13	0.87	2	–
	FPMD[d]	3.92	0	3.92	0.98	1.00	1.98	2.368
	FPMD ($N = 120$)[h]	3.96	0	3.96	0.99	0.99	1.98	2.376
	FPMD ($N = 480$)[h]	3.85	0.36	4.21	0.96	1.04	2	2.442
	FPMD ($N = 480$)[i]	3.96	0.04	4.00	0.99	1.01	2	2.4
	FPMD ($N = 480$)[j]	3.94	0.04	3.98	0.99	1.02	2.01	2.396
	CON	4	0	4	1	1	2	2.4
	RCN	8/3 = 2.667	4/3 = 1.333	4	2/3 = 0.667	4/3 = 1.333	2	2.4

The results from NDIS experiments are compared to those found from (i) the fractions of Se atoms in Se-Se-Se, Ge-Se-Se, or Ge-Se-Ge connections measured by using ^{77}Se NMR (section 5.1) or (ii) FPMD simulations (section 5.2). The predictions of the CON and RCN models are also listed (Salmon, 2007a). [a]Petri et al., 2000; Salmon and Petri, 2003 [b]Gjersing et al., 2010b [c]Kibalchenko et al., 2011 [d]Micoulaut et al., 2013 [e]Bouzid and Massobrio, 2012; Wezka et al., 2014 [f]Present work [g]Kaseman et al., 2016 [h]Bouzid et al., 2015 [i]vdW$_G$: Chaker et al., 2018 [j]vdW$_W$: Chaker et al., 2018.

$2(1 - 3x) / (1 - x)$, and $\bar{n}_{Ge}^{Ge} = 0$, whereas only Ge-Se and Ge-Ge bonds are allowed for compositions with $x > 1/3$ such that $\bar{n}_{Ge}^{Se} = 2(1 - x)/x$, $\bar{n}_{Se}^{Se} = 0$, and $\bar{n}_{Ge}^{Ge} = 2(3x - 1)/x$. By contrast, in the RCN there is a purely statistical distribution of bond types such that Se-Se bonds are allowed for $x > 1/3$ and Ge-Ge bonds are allowed for $x < 1/3$. In this case, the coordination numbers are given by $\bar{n}_{Ge}^{Se} = 4(1 - x)/(1 + x)$, $\bar{n}_{Se}^{Se} = 2(1 - x)/(1 + x)$ and $\bar{n}_{Ge}^{Ge} = 8x/(1 + x)$. **Table 2** shows that the coordination numbers from the NDIS method are consistent with the CON for GeSe$_3$ and GeSe$_4$, and that there is a breakdown of the chemical ordering for GeSe$_2$.
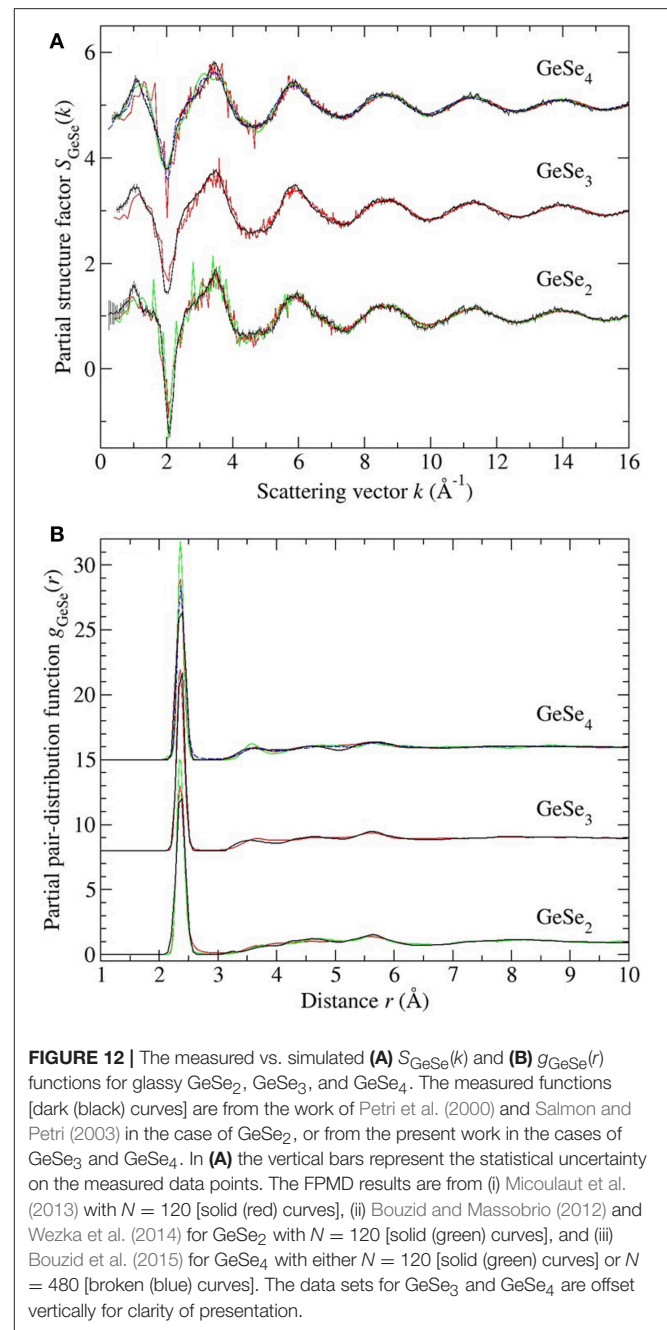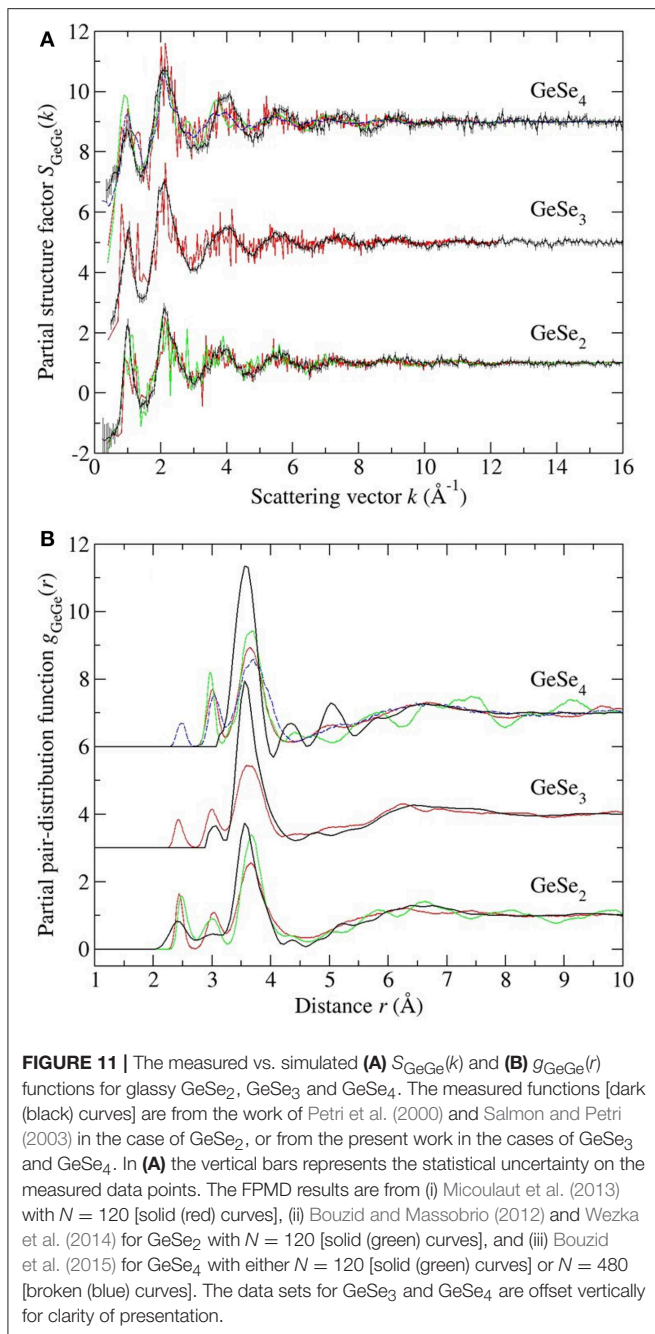
The fraction of Ge atoms in ES tetrahedral motifs can be estimated by assuming that there are no extended chains of ES motifs. Then, each ES conformation will involve two ES Ge atoms, two ES Se atoms and four other Se atoms, i.e., each ES Ge atom will be associated with one other ES Ge atom. The corresponding Ge-Ge coordination number is given by $\bar{n}_{Ge}^{Ge} = (N_{Ge,ES} / N_{Ge}) \times 1$, where $N_{Ge,ES}$ is the number of Ge atoms in ES motifs and N_{Ge} is the total number of Ge atoms in the glass. In order to make a quantitative comparison with the results from ^{77}Se MAS NMR experiments (Gjersing et al., 2010b), the fraction of Se atoms in ES Ge-Se-Ge connections needs to be estimated from the NDIS results. With the assumption that there are no extended chains of ES motifs, each pair of ES Ge atoms will be associated with two ES Se atoms, i.e., $N_{Ge,ES} = N_{Se,ES}$

such that $N_{Se,ES}/N_{Se} = (N_{Ge}/N_{Se}) \bar{n}_{Ge}^{Ge} = x \bar{n}_{Ge}^{Ge} / (1 - x)$. Hence, the measured NDIS $\bar{n}_{Ge}^{Ge}$ values give $N_{Se,ES} / N_{Se} = 0.17(3)$ for GeSe$_2$ vs. $N_{Se,ES} / N_{Se} = 0.05(2)$ for GeSe$_3$. In comparison, the ^{77}Se MAS NMR experiments give $N_{Se,ES} / N_{Se}$ values of 0.23(3) and 0.10(3) for GeSe$_2$ and GeSe$_{3.78}$, respectively. For the case of GeSe$_4$, there is no evidence of ES conformations from the NDIS experiments, although the low-r tail on the first peak in $g_{GeGe}(r)$ does cover part of the distance range expected for ES tetrahedra. In comparison, ^{77}Se MAS NMR experiments give $N_{Se,ES} / N_{Se} = 0.08(3)$ for GeSe$_4$ (Gjersing et al., 2010b), and Raman spectroscopy experiments report the existence of ES tetrahedra over the entire composition range $0.1 \leq x \leq 0.33$ (Sugai, 1987; Wang et al., 1998; Lucas et al., 2009; Gjersing et al., 2010b; Bhosle et al., 2012).

We note that the presence of ES conformations and the appearance of an FSDP in $S_{CC}(k)$ (**Figure 9**) are in contradiction with the chain-crossing model for Ge$_x$Se$_{1-x}$ glasses with $x < 1/3$ in which a uniform distribution of Ge-centered structural motifs is hypothesized (Tronc et al., 1973; Bureau et al., 2003).

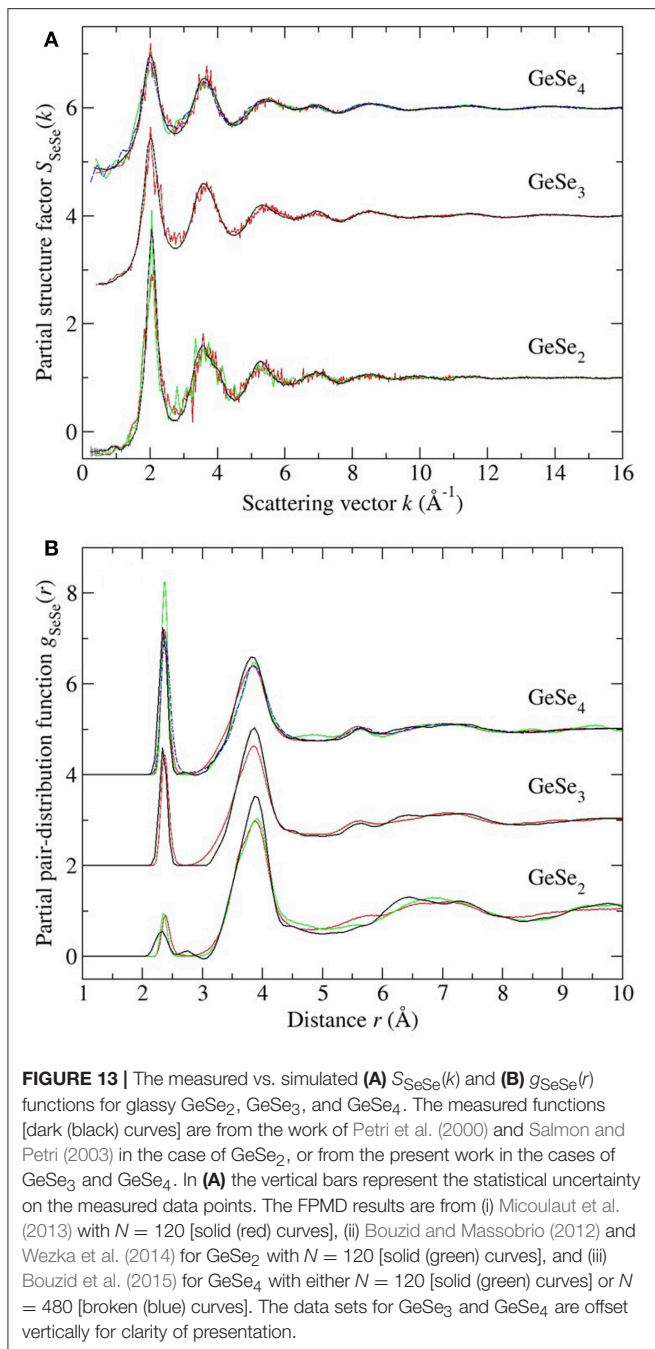## 5.2. Comparison With FPMD Models
In **Figures 11–13**, the measured $S_{\alpha\beta}(k)$ and $g_{\alpha\beta}(r)$ functions are compared to those obtained from $N = 120$ atom FPMD simulations of GeSe$_2$ (Bouzid and Massobrio, 2012; Micoulaut et al., 2013; Wezka et al., 2014), GeSe$_3$ (Micoulaut et al.,

FIGURE 11 | The measured vs. simulated **(A)** $S_{GeGe}(k)$ and **(B)** $g_{GeGe}(r)$ functions for glassy GeSe$_2$, GeSe$_3$ and GeSe$_4$. The measured functions [dark (black) curves] are from the work of Petri et al. (2000) and Salmon and Petri (2003) in the case of GeSe$_2$, or from the present work in the cases of GeSe$_3$ and GeSe$_4$. In **(A)** the vertical bars represents the statistical uncertainty on the measured data points. The FPMD results are from (i) Micoulaut et al. (2013) with $N = 120$ [solid (red) curves], (ii) Bouzid and Massobrio (2012) and Wezka et al. (2014) for GeSe$_2$ with $N = 120$ [solid (green) curves], and (iii) Bouzid et al. (2015) for GeSe$_4$ with either $N = 120$ [solid (green) curves] or $N = 480$ [broken (blue) curves]. The data sets for GeSe$_3$ and GeSe$_4$ are offset vertically for clarity of presentation.

FIGURE 12 | The measured vs. simulated **(A)** $S_{GeSe}(k)$ and **(B)** $g_{GeSe}(r)$ functions for glassy GeSe$_2$, GeSe$_3$, and GeSe$_4$. The measured functions [dark (black) curves] are from the work of Petri et al. (2000) and Salmon and Petri (2003) in the case of GeSe$_2$, or from the present work in the cases of GeSe$_3$ and GeSe$_4$. In **(A)** the vertical bars represent the statistical uncertainty on the measured data points. The FPMD results are from (i) Micoulaut et al. (2013) with $N = 120$ [solid (red) curves], (ii) Bouzid and Massobrio (2012) and Wezka et al. (2014) for GeSe$_2$ with $N = 120$ [solid (green) curves], and (iii) Bouzid et al. (2015) for GeSe$_4$ with either $N = 120$ [solid (green) curves] or $N = 480$ [broken (blue) curves]. The data sets for GeSe$_3$ and GeSe$_4$ are offset vertically for clarity of presentation.

2013), and GeSe$_4$ (Micoulaut et al., 2013; Bouzid et al., 2015) and from $N = 480$ atom simulations of GeSe$_4$ (Bouzid et al., 2015). In all of this FPMD work, the Becke-Lee-Yang-Parr (BLYP) exchange and correlation energy functional was employed (Becke, 1988; Lee et al., 1988), and steps were taken to ensure that the simulated systems were free from residual pressure (Bouzid and Massobrio, 2012). The simulated nearest-neighbor coordination numbers are compared to the measured values in **Table 2**.

Each model gives a good account of the measured Ge-Se and Se-Se correlation functions, but agreement with the measured Ge-Ge correlation functions is less impressive. In general, it is precisely the Ge-Ge correlations that show the greatest sensitivity to the details of the modeling procedure (Salmon and Zeidler, 2015), e.g., to the exchange and correlation energy functional used in the simulations (Massobrio et al., 1999, 2000, 2010; Micoulaut et al., 2009, 2013), to the effect on the structure of any residual pressure (Bouzid and Massobrio, 2012), and to the effect on the structure of both the system size and quench protocol that is employed, especially for small Ge content glasses (Bouzid et al., 2015; Le Roux et al., 2016).

FIGURE 13 | The measured vs. simulated **(A)** $S_{SeSe}(k)$ and **(B)** $g_{SeSe}(r)$ functions for glassy GeSe$_2$, GeSe$_3$, and GeSe$_4$. The measured functions [dark (black) curves] are from the work of Petri et al. (2000) and Salmon and Petri (2003) in the case of GeSe$_2$, or from the present work in the cases of GeSe$_3$ and GeSe$_4$. In **(A)** the vertical bars represent the statistical uncertainty on the measured data points. The FPMD results are from (i) Micoulaut et al. (2013) with $N = 120$ [solid (red) curves], (ii) Bouzid and Massobrio (2012) and Wezka et al. (2014) for GeSe$_2$ with $N = 120$ [solid (green) curves], and (iii) Bouzid et al. (2015) for GeSe$_4$ with either $N = 120$ [solid (green) curves] or $N = 480$ [broken (blue) curves]. The data sets for GeSe$_3$ and GeSe$_4$ are offset vertically for clarity of presentation.

In the case of GeSe$_2$, the models reproduce all of the measured features in $g_{GeGe}(r)$, although the CS tetrahedral peak at $\bar{r}_{GeGe} \sim 3.66$ Å is shifted toward a larger-r value as compared to experiment. In the case of GeSe$_3$, the model gives homonuclear Ge-Ge bonds in addition to ES and CS tetrahedral motifs, but homonuclear bonds were not found in the NDIS results, and the height of the CS peak in the simulated $g_{GeGe}(r)$ function is smaller than the measured value. In the case of GeSe$_4$, homonuclear Ge-Ge bonds were found in one FPMD model but not in the others, connections that were not found by experiment. Each

model features a clearly defined ES tetrahedral peak in $g_{GeGe}(r)$ at $\bar{r}_{GeGe} \sim 3.0$ Å that is absent in the measured function, although there is some overlap of the modeled ES peak with the low-r tail of the first peak in the measured $g_{GeGe}(r)$ function. The height of the CS peak in the simulated $g_{GeGe}(r)$ function is smaller than the measured value. These general findings from the NDIS experiments on GeSe$_3$ and GeSe$_4$ support those obtained from reverse Monte Carlo (RMC) models that were used to analyze the results obtained from anomalous X-ray scattering (AXS) experiments (Hosokawa et al., 2011).

The inclusion of dispersion or van der Waals (vdW) forces in FPMD simulations has recently been considered by Chaker et al. (2018) for the case of glassy GeSe$_4$. Two different theoretical schemes were used for the description of these forces, one based on the work of Grimme (2006) (vdW$_G$) and the other based on a Wannier function analysis (vdW$_W$) (Silvestrelli, 2008). The results were compared to those obtained for the $N = 480$ atom FPMD model of Bouzid et al. (2015) in which dispersion forces were not included. The main effect of dispersion forces is to (i) increase the height of the CS tetrahedral peak in $g_{GeGe}(r)$ at $\bar{r}_{GeGe} \simeq 3.6$ Å, making it comparable to the height found in the FPMD simulations of Micoulaut et al. (2013), and (ii) either leave constant or increase the height of the second peak in $g_{SeSe}(r)$ at $\bar{r}_{SeSe} \simeq 3.8$ Å, depending on the theoretical scheme. The dispersion corrections lead to $\bar{n}_{Ge}$ values that are in better accord with the "8-N" rule (**Table 2**).

5.3. Intermediate Phase

High-energy X-ray diffraction, neutron diffraction and EXAFS spectroscopy experiments have been performed to look for a structural signature of the intermediate phase in Ge$_x$Se$_{1-x}$ glass (Shatnawi et al., 2008; Zeidler et al., 2017). The composition dependence of several parameters was investigated across the stiffness transition. These parameters included descriptors of the local structure such as (i) the first peak position and width in the total pair-distribution function, (ii) the mean coordination number $\bar{n}$, and (iii) the Debye-Waller factor describing the root-mean-square displacement (static or thermal) of atoms about their equilibrium positions. They also included descriptors of the non-local structure on length scales that are associated with the FSDP and principal peak in the measured total structure factors, where ordering associated with the principal peak can persist to a nanometer length scale (Salmon et al., 2005; Salmon, 2006). All of these parameters were found to evolve smoothly with the glass composition, i.e., a structural signature of the intermediate phase was not identified.

The present work provides benchmark results for guiding in the development of accurate models for the structures of glassy GeSe$_3$ and GeSe$_4$, which can be used to explore the network rigidity and other structure-related properties of the glass. The investigated glasses lie at the boundaries of the intermediate phase in the Ge$_x$Se$_{1-x}$ system, which is reported for the composition range $0.20 \leq x \leq 0.26$ (section 1). Often, models for the glass structure are provided by FPMD simulations, and the onset of a stressed-rigid phase has been attributed to a substantial change in the distribution of bond

angles associated with Ge-centered tetrahedra, such that bond-angle constraints are broken for $x > 0.25$ (Micoulaut et al., 2013). However, as emphasized by the discussion of section 5.2, there is mismatch between the measured and FPMD results that is particularly noticeable in respect of the Ge-Ge correlation functions, which are sensitive to the connectivity of the Ge-centered structural motifs. In addition, different FPMD models can lead to different conclusions about the network structure. Thus, it will be interesting to see the predictions of FPMD models for intermediate phase glasses that are consistent with all of the measured partial pair-correlation functions.

6. CONCLUSIONS

Full sets of partial structure factors for glassy GeSe$_3$ ($x = 0.25$) and GeSe$_4$ ($x = 0.20$) were measured by using the NDIS method. These glass compositions lie at the boundaries of the intermediate phase in the Ge$_x$Se$_{1-x}$ system. The results are consistent with chemically ordered network structures, in contrast to GeSe$_2$ where the chemical ordering is broken by the formation of homonuclear Ge-Ge and Se-Se bonds (Petri et al., 2000; Salmon and Petri, 2003). For all of these compositions, the nearest-neighbor Ge and Se coordination numbers are given by $\bar{n}_{Ge} = 4$ and $\bar{n}_{Se} = 2$ within the experimental error (**Table 2**), in accordance with the expectations of the "8-N" rule. In the case of GeSe$_4$, larger $\bar{n}_{Ge}$ values are deduced from ^{77}Se MAS NMR experiments (**Table 2**), which suggests the need for a re-interpretation of the spectroscopy results. A distinct peak in $g_{GeGe}(r)$ at $\bar{r}_{GeGe} \sim 3.03$ Å that originates from ES tetrahedra was observed for both GeSe$_2$ and GeSe$_3$, but was not found for GeSe$_4$. This finding appears to contradict the results obtained from both ^{77}Se MAS NMR (Gjersing et al., 2010b) and Raman spectroscopy (Sugai, 1987; Wang et al., 1998; Lucas et al., 2009; Gjersing et al., 2010b; Bhosle et al., 2012) experiments, although the low-r tail on the first peak in the measured $g_{GeGe}(r)$ function does have a contribution in the distance range associated with ES tetrahedra. The appearance of an FSDP in $S_{CC}(k)$ indicates a non-uniform distribution of Ge-centered tetrahedra on an intermediate length scale, in contradiction to the chain-crossing model (Tronc et al., 1973; Bureau et al., 2003).

The new experimental work provides benchmark results for aiding in the development of realistic structural models for establishing the network rigidity and other structure-related properties of the glass. A comparison of the NDIS results for GeSe$_3$ and GeSe$_4$ with those from recent FPMD simulations shows mismatch that is particularly marked in respect of the Ge-Ge correlation functions, i.e., there is an ingredient missing from the FPMD simulations that may be related to the system size.

DATA AVAILABILITY

The data sets created during this research are openly available from the University of Bath Research Data Archive at https://doi.org/10.15125/BATH-00664 (Salmon and Zeidler, 2019). Raw neutron diffraction data sets for GeSe$_3$ and GeSe$_4$ are available at https://doi.ill.fr/10.5291/ILL-DATA.6-05-922 (Salmon et al., 2013).

AUTHOR CONTRIBUTIONS

PSS and AZ designed the research. AZ prepared the samples. All authors contributed to the neutron diffraction experiments. RFR and AZ analyzed the data. PSS wrote the paper.

FUNDING

ACKNOWLEDGMENTS

REFERENCES

Bauchy, M., Micoulaut, M., Celino, M., Le Roux, S., Boero, M., and Massobrio, C. (2011). Angular rigidity in tetrahedral network glasses with changing composition. *Phys. Rev. B* 84:054201. doi: 10.1103/PhysRevB.84.054201

Becke, A. D. (1988). Density-functional exchange-energy approximation with correct asymptotic behavior. *Phys. Rev. A* 38, 3098–3100. doi: 10.1103/PhysRevA.38.3098

Bertagnolli, H., Chieux, P., and Zeidler, M. D. (1976). A neutron-diffraction study of liquid acetonitrile I. CD$_3$C^{14}N. *Mol. Phys.* 32, 759–773. doi: 10.1080/00268977600102201

Bhatia, A. B., and Thornton, D. E. (1970). Structural aspects of the electrical resistivity of binary alloys. *Phys. Rev. B* 2, 3004–3012. doi: 10.1103/PhysRevB.2.3004

Bhosle, S., Gunasekera, K., Boolchand, P., and Micoulaut, M. (2012). Melt homogenization and self-organization in chalcogenides - part II. *Int. J. Appl. Glass Sci.* 3, 205–220. doi: 10.1111/j.2041-1294.2012.00092.x

Bhosle, S., Gunasekera, K., Chen, P., Boolchand, P., Micoulaut, M., and Massobrio, C. (2011). Meeting experimental challenges to physics of network glasses: assessing the role of sample homogeneity. *Solid State Commun.* 151, 1851–1855. doi: 10.1016/j.ssc.2011.10.016

Boolchand, P., Feng, X., and Bresser, W. J. (2001a). Rigidity transitions in binary Ge-Se glasses and the intermediate phase. *J. Non-Cryst. Solids* 293–295, 348–356. doi: 10.1016/S0022-3093(01)00867-5

Boolchand, P., Georgiev, D. G., and Goodman, B. (2001b). Discovery of the intermediate phase in chalcogenide glasses. *J. Optoelectron. Adv. Mater.* 3, 703–720.

Bouzid, A., Le Roux, S., Ori, G., Boero, M., and Massobrio, C. (2015). Origin of structural analogies and differences between the atomic structures of GeSe$_4$ and GeS$_4$ glasses: A first principles study. *J. Chem. Phys.* 143:034504. doi: 10.1063/1.4926830

Bouzid, A., and Massobrio, C. (2012). Note: accounting for pressure effects on the calculated equilibrium structure of glassy GeSe$_2$. *J. Chem. Phys.* 137:046101. doi: 10.1063/1.4739953

Bresser, W., Boolchand, P., and Suranyi, P. (1986). Rigidity percolation and molecular clustering in network glasses. *Phys. Rev. Lett.* 56, 2493–2496. doi: 10.1103/PhysRevLett.56.2493

Bureau, B., Troles, J., Floch, M. L., Guénot, P., Smektala, F., and Lucas, J. (2003). Germanium selenide glass structures studied by ^{77}Se solid state NMR and mass spectroscopy. *J. Non-Cryst. Solids* 319, 145–153. doi: 10.1016/S0022-3093(02)01911-7

Chaker, Z., Ori, G., Tugène, C., Le Roux, S., Boero, M., Massobrio, C., et al. (2018). The role of dispersion forces on the atomic structure of glassy chalcogenides: the case of GeSe$_4$ and GeS$_4$. *J. Non-Cryst. Solids* 499, 167–172. doi: 10.1016/j.jnoncrysol.2018.07.012

Dittmar, G., and Schäfer, H. (1976). Die kristallstruktur von Germaniumdiselenid. *Acta Crystallogr. B* 32, 2726–2728. doi: 10.1107/S0567740876008704

Eggleton, B. J., Luther-Davies, B., and Richardson, K. (2011). Chalcogenide photonics. *Nat. Photon.* 5, 141–148. doi: 10.1038/nphoton.2011.309

Faber, T. E., and Ziman, J. M. (1965). A theory of the electrical properties of liquid metals. III. The resistivity of binary alloys. *Philos. Mag.* 11, 153–173. doi: 10.1080/14786436508211931

Feng, X., Bresser, W. J., and Boolchand, P. (1997). Direct evidence for stiffness threshold in chalcogenide glasses. *Phys. Rev. Lett.* 78, 4422–4425. doi: 10.1103/PhysRevLett.78.4422

Fischer, H. E., Barnes, A. C., and Salmon, P. S. (2006). Neutron and x-ray diffraction studies of liquids and glasses. *Rep. Prog. Phys.* 69, 233–299. doi: 10.1088/0034-4885/69/1/R05

Fischer, H. E., Cuello, G. J., Palleau, P., Feltin, D., Barnes, A. C., Badyal, Y. S., et al. (2002). D4c: A very high precision diffractometer for disordered materials. *Appl. Phys. A* 74, S160–S162. doi: 10.1007/s003390101087

Gjersing, E. L., Sen, S., and Youngman, R. E. (2010a). Mechanistic understanding of the effect of rigidity percolation on structural relaxation in supercooled germanium selenide liquids. *Phys. Rev. B* 82:014203. doi: 10.1103/PhysRevB.82.014203

Gjersing, E. L., Sen, S., and Youngman, R. E. (2010b). Structure, connectivity, and configurational entropy of Ge$_x$Se$_{100-x}$ glasses: Results from ^{77}Se MAS NMR spectroscopy. *J. Phys. Chem. C* 114, 8601–8608. doi: 10.1021/jp1014143

Gopinath, J. T., Soljačić, M., Ippen, E. P., Fuflyigin, V. N., King, W. A., and Shurgalin, M. (2004). Third order nonlinearities in Ge-As-Se-based glasses for telecommunications applications. *J. Appl. Phys.* 96, 6931–6933. doi: 10.1063/1.1805182

Grimme, S. (2006). Semiempirical GGA-type density functional constructed with a long-range dispersion correction. *J. Comput. Chem.* 27, 1787–1799. doi: 10.1002/jcc.20495

Hilton, A. R. (1966). Nonoxide chalcogenide glasses as infrared optical materials. *Appl. Opt.* 5, 1877–1882. doi: 10.1364/AO.5.001877

Hosokawa, S., Oh, I., Sakurai, M., Pilgrim, W.-C., Boudet, N., Bérar, J.-F., et al. (2011). Anomalous x-ray scattering study of Ge$_x$Se$_{1-x}$ glassy alloys across the stiffness transition composition. *Phys. Rev. B* 84:014201. doi: 10.1103/PhysRevB.84.014201

Inam, F., Tafen, D. N., Chen, G., and Drabold, D. A. (2009). Competing stoichiometric phases and the intermediate phase in Ge$_x$Se$_{1-x}$ glasses. *Phys. Stat. Solid B* 246, 1849–1853. doi: 10.1002/pssb.200982016

Kaseman, D. C., Oliveira, K. M., Palazzo, T., and Sen, S. (2016). Selenium chain length distribution in Ge$_x$Se$_{100-x}$ glasses: insights from ^{77}Se NMR spectroscopy and quantum chemical calculations. *J. Phys. Chem. B* 120, 4513–4521. doi: 10.1021/acs.jpcb.6b02747

Kibalchenko, M., Yates, J. R., Massobrio, C., and Pasquarello, A. (2011). Structural composition of first-neighbor shells in GeSe$_2$ and GeSe$_4$ glasses from a first-principles analysis of NMR chemical shifts. *J. Phys. Chem. C* 115, 7755–7759. doi: 10.1021/jp201345e

Kohoutek, T., Wagner, T., Orava, J., Krbal, M., Ilavsky, J., Vlcek, M., et al. (2008). Multilayer planar structures prepared from chalcogenide thin films of As-Se and Ge-Se systems and polymer thin films using thermal evaporation and spin-coating techniques. *J. Non-Cryst. Solids* 354, 529–532. doi: 10.1016/j.jnoncrysol.2007.07.057

Le Roux, S., Bouzid, A., Kim, K. Y., Han, S., Zeidler, A., Salmon, P. S., et al. (2016). Structure of amorphous GeSe$_9$ by neutron diffraction and first-principles molecular dynamics: impact of trajectory sampling and size effects. *J. Chem. Phys.* 145:084502. doi: 10.1063/1.4961265

Lee, C., Yang, W., and Parr, R. G. (1988). Development of the Colle-Salvetti correlation-energy formula into a functional of the electron density. *Phys. Rev. B* 37, 785–789. doi: 10.1103/PhysRevB.37.785

Lezal, D., Pedlikova, J., and Zavadil, J. (2004). Chalcogenide glasses for optical and photonics applications. *J. Optoelectron. Adv. Mater.* 6, 133–137.

Lorch, E. (1969). Neutron diffraction by germania, silica and radiation-damaged silica glasses. *J. Phys. C Solid State Phys.* 2, 229–237. doi: 10.1088/0022-3719/2/2/305

Lucas, P., Coleman, G. J., Sen, S., Cui, S., Guimond, Y., Calvez, L., et al. (2019). Structural and chemical homogeneity of chalcogenide glass prepared by melt-rocking. *J. Chem. Phys.* 150:014505. doi: 10.1063/1.5054704

Lucas, P., King, E. A., Gulbiten, O., Yarger, J. L., Soignard, E., and Bureau, B. (2009). Bimodal phase percolation model for the structure of Ge-Se glasses and the existence of the intermediate phase. *Phys. Rev. B* 80:214114. doi: 10.1103/PhysRevB.80.214114

Ludwig, K. F. Jr., Warburton, W. K., Wilson, L., and Bienenstock, A. I. (1987). Liquid GeBr$_4$. I. A test of the anomalous x-ray scattering method as applied to disordered materials. *J. Chem. Phys.* 87, 604–612. doi: 10.1063/1.453553

Madon, M., Gillet, P., Julien, C., and Price, G. D. (1991). A vibrational study of phase transitions among the GeO$_2$ polymorphs. *Phys. Chem. Miner.* 18, 7–18. doi: 10.1007/BF00199038

Martin, R. A., Salmon, P. S., Fischer, H. E., and Cuello, G. J. (2003). Structure of dysprosium and holmium phosphate glasses by the method of isomorphic substitution in neutron diffraction. *J. Phys. Condens. Matter* 15, 8235–8252. doi: 10.1088/0953-8984/15/49/003

Massobrio, C., Celino, M., Salmon, P. S., Martin, R. A., Micoulaut, M., and Pasquarello, A. (2009). Atomic structure of the two intermediate phase glasses SiSe$_4$ and GeSe$_4$. *Phys. Rev. B* 79:174201. doi: 10.1103/PhysRevB.79.174201

Massobrio, C., Micoulaut, M., and Salmon, P. S. (2010). Impact of the exchange-correlation functional on the structure of glassy GeSe$_2$. *Solid State Sci.* 12, 199–203. doi: 10.1016/j.solidstatesciences.2009.11.016

Massobrio, C., Pasquarello, A., and Car, R. (1999). Intermediate range order and bonding character in disordered network-forming systems. *J. Am. Chem. Soc.* 121, 2943–2944. doi: 10.1021/ja9808447

Massobrio, C., Pasquarello, A., and Car, R. (2000). Concentration fluctuations on intermediate range distances in liquid GeSe$_2$: the critical role of ionicity. *Comput. Mater. Sci.* 17, 115–121. doi: 10.1016/S0927-0256(00)00007-0

Micoulaut, M., Cormier, L., and Henderson, G. S. (2006). The structure of amorphous, crystalline and liquid GeO$_2$. *J. Phys. Condens. Matter* 18, R753–R784. doi: 10.1088/0953-8984/18/45/R01

Micoulaut, M., Kachmar, A., Bauchy, M., Le Roux, S., Massobrio, C., and Boero, M. (2013). Structure, topology, rings, and vibrational and electronic properties of Ge$_x$Se$_{1-x}$ glasses across the rigidity transition: a numerical study. *Phys. Rev. B* 88:054203. doi: 10.1103/PhysRevB.88.054203

Micoulaut, M., Vuilleumier, R., and Massobrio, C. (2009). Improved modeling of liquid GeSe$_2$: impact of the exchange-correlation functional. *Phys. Rev. B* 79:214205. doi: 10.1103/PhysRevB.79.214205

Penfold, I. T., and Salmon, P. S. (1991). Structure of covalently bonded glass-forming melts: a full partial-structure-factor analysis of liquid GeSe$_2$. *Phys. Rev. Lett.* 67, 97–100. doi: 10.1103/PhysRevLett.67.97

Petri, I., Salmon, P. S., and Fischer, H. E. (1999a). Structure of the liquid semiconductor GeSe. *J. Phys. Condens. Matter* 11, 7051–7060. doi: 10.1088/0953-8984/11/37/302

Petri, I., Salmon, P. S., and Fischer, H. E. (2000). Defects in a disordered world: the structure of glassy GeSe$_2$. *Phys. Rev. Lett.* 84, 2413–2416. doi: 10.1103/PhysRevLett.84.2413

Petri, I., Salmon, P. S., and Howells, W. S. (1999b). Change in the topology of the glass forming liquid GeSe$_2$ with increasing temperature. *J. Phys. Condens. Matter* 11, 10219–10227. doi: 10.1088/0953-8984/11/50/314

Phillips, J. C. (1979). Topology of covalent non-crystalline solids I: short-range order in chalcogenide alloys. *J. Non-Cryst. Solids* 34, 153–181. doi: 10.1016/0022-3093(79)90033-4

Rowlands, R. F. (2015). *The role of structural disorder in crystalline, glassy and liquid materials.* (Ph.D. thesis), University of Bath, Bath, United Kingdom.

Salmon, P. S. (1992). The structure of molten and glassy 2:1 binary systems: an approach using the Bhatia-Thornton formalism. *Proc. R. Soc. Lond. A* 437, 591–606. doi: 10.1098/rspa.1992.0081

Salmon, P. S. (1994). Real space manifestation of the first sharp diffraction peak in the structure factor of liquid and glassy materials. *Proc. R. Soc. Lond. A* 445, 351–365. doi: 10.1098/rspa.1994.0065

Salmon, P. S. (2006). Decay of the pair correlations and small-angle scattering for binary liquids and glasses. *J. Phys. Condens. Matter* 18, 11443–11469. doi: 10.1088/0953-8984/18/50/004

Salmon, P. S. (2007a). Structure of liquids and glasses in the Ge-Se binary system. *J. Non-Cryst. Solids* 353, 2959–2974. doi: 10.1016/j.jnoncrysol.2007.05.152

Salmon, P. S. (2007b). The structure of tetrahedral network glass forming systems at intermediate and extended length scales. *J. Phys. Condens. Matter* 19:455208. doi: 10.1088/0953-8984/19/45/455208

Salmon, P. S., Fischer, H. E., Rowlands, R. F., and Zeidler, A. (2013). Structure of intermediate phase glasses. doi: 10.5291/ILL-DATA.6-05-922

Salmon, P. S., and Liu, J. (1994). The relation between the melt topology and glass-forming ability for liquid Ge-Se alloys. *J. Phys. Condens. Matter* 6, 1449–1460. doi: 10.1088/0953-8984/6/8/004

Salmon, P. S., Martin, R. A., Mason, P. E., and Cuello, G. J. (2005). Topological vs. chemical ordering in network glasses at intermediate and extended length scales. *Nature* 435, 75–78. doi: 10.1038/nature03475

Salmon, P. S., and Petri, I. (2003). Structure of glassy and liquid GeSe$_2$. *J. Phys. Condens. Matter* 15, S1509–S1528. doi: 10.1088/0953-8984/15/16/301

Salmon, P. S., Xin, S., and Fischer, H. E. (1998). Structure of the glassy fast-ion conductor AgPS$_3$ by neutron diffraction. *Phys. Rev. B* 58, 6115–6123. doi: 10.1103/PhysRevB.58.6115

Salmon, P. S., and Zeidler, A. (2013). Identifying and characterising the different structural length scales in liquids and glasses: an experimental approach. *Phys. Chem. Chem. Phys.* 15, 15286–15308. doi: 10.1039/c3cp51741a

Salmon, P. S., and Zeidler, A. (2015). "Chapter 1: The atomic-scale structure of network glass-forming materials," in *Molecular Dynamics Simulations of Disordered Materials*, Springer Series in Materials Science 215, eds C. Massobrio, J. Du, M. Bernasconi, and P. S. Salmon (Cham: Springer), 1–31. doi: 10.1007/978-3-319-15675-0_1

Salmon, P. S. and Zeidler, A. (2019). Data sets for the Frontiers in Materials article entitled "Structure of Ge-Se glass and network rigidity: The deployment of neutron diffraction with isotope substitution". doi: 10.15125/BATH-00664

Salmon, P. S., Zeidler, A., and Fischer, H. E. (2016). Optimizing the counting times for sample-in-container scattering experiments. *J. Appl. Cryst.* 49, 2249–2251. doi: 10.1107/S160057671601493X

Sartbaeva, A., Wells, S. A., Huerta, A., and Thorpe, M. F. (2007). Local structural variability and the intermediate phase window in network glasses. *Phys. Rev. B* 75:224204. doi: 10.1103/PhysRevB.75.224204

Savage, J. A., and Nielsen, S. (1965). Chalcogenide glasses transmitting in the infrared between 1 and 20 µ - a state of the art review. *Infrared Phys.* 5, 195–204. doi: 10.1016/0020-0891(65)90023-0

Sears, V. F. (1992). Neutron scattering lengths and cross sections. *Neutron News* 3, 26–37. doi: 10.1080/10448639208218770

Seddon, A. B., and Laine, M. J. (1997). Chalcogenide glasses for acousto-optic devices. II. As-Ge-Se systems. *J. Non-Cryst. Solids* 213–214, 168–173. doi: 10.1016/S0022-3093(96)00665-5

Shatnawi, M. T. M., Farrow, C. L., Chen, P., Boolchand, P., Sartbaeva, A., Thorpe, M. F., et al. (2008). Search for a structural response to the intermediate phase in Ge$_x$Se$_{1-x}$ glasses. *Phys. Rev. B* 77:094134. doi: 10.1103/PhysRevB.77.094134

Silvestrelli, P. L. (2008). Van der Waals interactions in DFT made easy by Wannier functions. *Phys. Rev. Lett.* 100:053002. doi: 10.1103/PhysRevLett.100.053002

Sugai, S. (1987). Stochastic random network model in Ge and Si chalcogenide glasses. *Phys. Rev. B* 35, 1345–1361. doi: 10.1103/PhysRevB.35.1345

Thorpe, M. F. (1983). Continuous deformations in random networks. *J. Non-Cryst. Solids* 57, 355–370. doi: 10.1016/0022-3093(83)90424-6

Thorpe, M. F., Jacobs, D. J., Chubynsky, M. V., and Phillips, J. C. (2000). Self-organization in network glasses. *J. Non-Cryst. Solids* 266–269, 859–866. doi: 10.1016/S0022-3093(99)00856-X

Troles, J., Shiryaev, V., Churbanov, M., Houizot, P., Brilland, L., Desevedavy, F., et al. (2009). GeSe$_4$ glass fibres with low optical losses in the mid-IR. *Opt. Mater.* 32, 212–215. doi: 10.1016/j.optmat.2009.07.024

Tronc, P., Bensoussan, M., Brenac, A., and Sebenne, C. (1973). Optical-absorption edge and Raman scattering in Ge$_x$Se$_{1-x}$ glasses. *Phys. Rev. B* 8, 5947–5956. doi: 10.1103/PhysRevB.8.5947

Wang, Y., Matsuda, O., Inoue, K., Yamamuro, O., Matsuo, T., and Murase, K. (1998). A Raman scattering investigation of the structure of glassy and liquid Ge$_x$Se$_{1-x}$. *J. Non-Cryst. Solids* 232-234, 702–707. doi: 10.1016/S0022-3093(98)00553-5

Wezka, K., Bouzid, A., Pizzey, K. J., Salmon, P. S., Zeidler, A., Klotz, S., et al. (2014). Density-driven defect-mediated network collapse of GeSe$_2$ glass. *Phys. Rev. B* 90:054206. doi: 10.1103/PhysRevB.90.054206

Whittaker, D. A. J., Giacomazzi, L., Adroja, D., Bennington, S. M., Pasquarello, A., and Salmon, P. S. (2018). Partial vibrational density of states for amorphous solids from inelastic neutron scattering. *Phys. Rev. B* 98:064205. doi: 10.1103/PhysRevB.98.064205

Wright, A. C. (1993). The comparison of molecular dynamics simulations with diffraction experiments. *J. Non-Cryst. Solids* 159, 264–268. doi: 10.1016/0022-3093(93)90232-M

Zakery, A., and Elliott, S. R. (2003). Optical properties and applications of chalcogenide glasses: a review. *J. Non-Cryst. Solids* 330, 1–12. doi: 10.1016/j.jnoncrysol.2003.08.064

Zakery, A., and Elliott, S. R. (2007). *Optical Nonlinearities in Chalcogenide Glasses and Their Applications*. Springer Series in Optical Sciences 135. Berlin: Springer. doi: 10.1007/978-3-540-71068-4

Zeidler, A., Salmon, P. S., Fischer, H. E., Neuefeind, J. C., Simonson, J. M., and Markland, T. E. (2012). Isotope effects in water as investigated by neutron diffraction and path integral molecular dynamics. *J. Phys. Condens. Matter* 24:284126. doi: 10.1088/0953-8984/24/28/284126

Zeidler, A., Salmon, P. S., Martin, R. A., Usuki, T., Mason, P. E., Cuello, G. J., et al. (2010). Structure of liquid and glassy ZnCl$_2$. *Phys. Rev. B* 82:104208. doi: 10.1103/PhysRevB.82.104208

Zeidler, A., Salmon, P. S., Whittaker, D. A. J., Pizzey, K. J., and Hannon, A. C. (2017). Topological ordering and viscosity in the glass-forming Ge-Se system: the search for a structural or dynamical signature of the intermediate phase. *Front. Mater.* 4:32. doi: 10.3389/fmats.2017.00032

Zhou, W., Paesler, M., and Sayers, D. E. (1991). Structure of germanium-selenium glasses: an X-ray-absorption fine-structure study. *Phys. Rev. B* 43, 2315–2321. doi: 10.1103/PhysRevB.43.2315